*J. Fluid Mech.* (2002), *vol.* 466, *pp.* 113–147. © 2002 Cambridge University Press
DOI: 10.1017/S0022112002001210 Printed in the United Kingdom


# The linear stability of a core–annular flow in an asymptotically corrugated tube

By HSIEN-HUNG WEI AND DAVID S. RUMSCHITZKI

Department of Chemical Engineering, City College of CUNY,
140th Street at Convent Avenue, New York, NY 10031, USA
and Graduate School and University Center CUNY, New York, NY 10016, USA

(Received 2 February 2001 and in revised form 23 January 2002)

This paper examines the core–annular flow of two immiscible fluids in a straight circular tube with a small corrugation, in the limit where the ratio $\varepsilon$ of the mean undisturbed annulus thickness to the mean core radius and the corrugation (characterized by the parameter $\sigma$) are both asymptotically small and where the surface tension is small. It is motivated by the problems of liquid–liquid displacement in irregular rock pores such as occur in secondary oil recovery and in the evolution of the liquid film lining the bronchii in the lungs whose diameters vary over different generations of branching. We investigate the asymptotic base flow in this limit and consider the linear stability of its leading order (in the corrugation parameter) solution. For the chosen scalings of the non-dimensional parameters the core's base flow slaves that of the annulus. The equation governing the leading-order interfacial position for a given wall corrugation function shows a competition between shear and capillarity. The former tends to align the interface shape with that of the wall and the latter tends to introduce a phase shift, which can be of either sign depending on whether the circumferential or the longitudinal component of capillarity dominates.

The asymptotic linear stability of this leading-order base flow reduces to a single partial differential equation with non-constant coefficients deriving from the non-uniform base flow for the time evolution of an interfacial disturbance. Examination of a single mode $k$ wall function allows the use of Floquet theory to analyse this equation. Direct numerical solutions of the above partial differential equation agree with the predictions of the Floquet analysis. The resulting spectrum is periodic in $\alpha$-space, $\alpha$ being the disturbance wavenumber space. The presence of a small corrugation not only modifies (at order $\sigma^2$) the primary eigenvalue of the system. In addition, short-wave order-one disturbances that would be stabilized owing to capillarity in the absence of corrugation can, in the presence of corrugation and over time scales of order $\ln(1/\sigma)$, excite higher wall harmonics ($\alpha \pm nk$) leading to the growth of unstable long waves. Similar results obtain for more complicated wall shape functions. The main result is that a small corrugation makes a core–annular flow unstable to far more disturbances than would destabilize the same uncorrugated flow system. A companion paper examines that competition between this added destabilization due to pore corrugation with the wave steepening and stabilization in the weakly nonlinear regime.

## 1. Introduction

A two-fluid core–annular flow (CAF) consists of two immiscible fluids flowing cocurrently in a tube or pore, where one (the annular) fluid wets the tube wall and

surrounds the other (core) fluid. Core–annular flows are widely studied and employed as a useful model to analyse a number of technologies and problems of scientific and technological interest such as secondary oil recovery (Slattery 1974), liquid–liquid displacements in porous media (Park & Homsy 1984), lubricated piping (Preziosi, Chen & Joseph 1989), and the lung surfactant problem (Halpern & Grotberg 1993; Otis *et al.* 1993). To recover oil that is saturating capillary pores in rocks, one can try to displace the oil with a second, immiscible liquid, usually an aqueous solution with low interfacial tension with the oil (Slattery 1974). If the displacing fluid is less viscous, it will finger into the extant fluid, which sticks to the pore wall owing to its non-slip condition there (Saffman & Taylor 1958). This creates a CAF away from the ends of the finger. An interfacial instability, however, can significantly affect the efficiency of the recovery process. Growing interfacial disturbances can cause the wetting layer to snap and bring the non-wetting phase in contact with the capillary pore wall. Contact line forces attaching the slug to the wall can retard train mobility, thereby making recovery more difficult. In addition, the pore's structure may significantly destablize the system since the uneven boundaries may potentially change the flow pattern dramatically and excite instability. In the lung, air travels through a hierarchy of branching tubes, called branchioles, whose inner surfaces are coated by a thin layer of fluid. This cylindrical liquid layer typically maintains its integrity during respiration owing to a surfactant produced in the lungs called DPPC, which retards the growth of the capillary instability to a time scale that is long compared with the breathing cycle. In premature infants and adults with adult respiration distress syndrome (ARDS), this surfactant is not present or does not function properly, and the core can become blocked, destroying the CAF and inhibiting respiration. Obviously, whether the flow is stable or not is relevant to the proper functioning of these systems.

It is important to understand the mechanism of instability in CAFs because it is often critical to either encourage or discourage the growth of the instability. It is not surprising that there are numerous investigations based on a perfect CAF (PCAF – perfect meaning coaxial and axisymmetric) through the idealized geometry of a straight, cylindrical tube. In these studies, the base flow for a PCAF is a Poiseuille flow field with a purely circular cylindrical interface, which satisfies the Navier–Stokes equation and the appropriate boundary conditions exactly. The dominant effects that influence the linear stability of a CAF are capillarity and viscosity stratification. Capillarity acts in two ways: it destabilizes the interfacial circumferential curvature and stabilizes the axial curvature of an interfacial deflection. The competition is such that disturbances with wavelengths shorter than the undisturbed interfacial circumference are stable and those with longer wavelengths are unstable. This feature of capillarity is independent of the base flow, and arises simply from the cylindrical geometry of the unperturbed fluid–fluid interface.

In the presence of a base flow, Hickox (1971) used Yih's long wavelength technique to examine the linear stability of a CAF with a more viscous film fluid ($m \equiv \mu_2/\mu_1 > 1$, $\mu_1$ and $\mu_2$ being the viscosities of the core and annular fluids, respectively) in the presence of capillarity, viscosity and density stratification and gravity in a vertical tube. In his analysis, for both axisymmetric and non-axisymmetric disturbances, both capillarity and viscosity stratification were destabilizing for long waves (to the leading order in wave number $\alpha$) and axisymmetric modes were the most unstable. Joseph and coworkers, in a series of papers (Joseph, Renardy & Renardy 1984; Preziosi, Chen & Joseph 1989; Hu & Joseph 1989; Chen, Bai & Joseph 1990; Hu, Lundgren & Joseph 1990; Chen & Joseph 1991), extensively investigated the combination of capillarity and viscosity stratification, for $m < 1$, for which the latter effect is

stabilizing. They numerically solved the full Orr–Sommerfeld equation and employed perturbation techniques, e.g. for small $m \ll 1$ in their analyses. In lubricated pipelining, $m < 1$ and viscosity stratification can stabilize the destabilization of capillarity for a band of Reynolds numbers. As such, they showed that there exists a window of stability in Reynolds number space in which a CAF is linearly stable. Such a window disappears when the film become too thick or when enhancing the film's viscosity relative to that of the core. In most applications, the thickness of the annular fluid is typically much smaller than the tube radius. In such cases, Georgiou *et al.* (1992) developed thin-film asymptotic techniques to examine analytically the linear stability of a PCAF in a vertical arrangement with gravity. They focused on axisymmetric, i.e. the most unstable, disturbances and extended Hickox's $\alpha \to 0$ analysis to the range of intermediate waves, i.e. waves comparable to the tube circumference. For large surface tensions and for $m < 1$, viscosity stratification can stabilize the capillary instability to the leading order in the ratio $\varepsilon$ of the undisturbed annular thickness to the core radius, while viscosity stratification is linearly destabilizing for $m > 1$. A density difference is purely dispersive to the leading order in $\varepsilon$ and its stability contribution is a second-order effect. In particular, the linear stability is primarily dominated by the fluid–fluid interfacial tension, i.e. capillarity, and viscosity stratification.

However, in a real core–annular flow systems such as occur in secondary oil recovery, two fluids flow through uneven channels in the porous rock and thus do not possess an ideal geometry as in a perfectly cylindrical tube. Similarly, the extensive branching of the bronchiole system represents a system with a frequently changing cross-section. It is thus conceivable that pore corrugation may play a role in determining the stability of the system that is at least as important as the effects that have already been considered (Wei & Rumschitzki 2002). However there are good reasons why one might neglect it in a first analysis. First, such geometric non-idealities will change the base state significantly. Even in an axisymmetric tube of varying cross-section, the base flow will be two-dimensional, rather than simply an axial velocity as a function of the radial position. This deviation from parallel flow can interact strongly with the disturbance introduced in the stability analysis. For instance, consider the flow of a single fluid in a sinusoidal tube. Even for small $Re$, inertia can become significant when the axial variation of the tube radius $\mathrm{d}R/\mathrm{d}z$ is as rapid as $O(1/Re)$. Moreover, it is unlikely that one would be able to solve for the base state, the starting point for a stability analysis, exactly in closed form. Cylindrical tube theory clearly does not include these effects. To access them, it is necessary to extend the scope of this theory to include these varying geometry factors.

There have been several studies of base flows in corrugated systems without an accompanying stability analysis. Simple systems such as a single fluid flowing in a tube or channel with varying cross-section (Chow & Soda 1972) have been studied. These works employ perturbation techniques, by using either small corrugation or slow axial variation parameters, for flows at intermediate or high Reynolds numbers. Similar techniques have been applied in interfacial problems. Wang (1981) considered a film flowing slowly down a wavy inclined plate where the striations are parallel to the overall flow. He applied a perturbation method with respect to the small amplitude of the corrugation and found that, for a fixed mean depth of the film, the flow transverse to the striations is decreased relative to that on a smooth plate, whereas the flow along the striations is increased. Dassori, Deiber & Cassano (1984) analysed a two-fluid system in a symmetrically sinusoidal, two-dimensional channel. They only focused on the case of a wetting fluid layer with very low density and viscosity relative to the core. Both of these studies found that the fluid interface

exhibited a wavy shape characterized by an amplitude and a phase shift relative to the wall, which are functions of the surface tension, the density ratio, viscosity stratification, the flow rate and the wavenumber of the wall. Recently, Kang & Chen (1995) extended Wang's analysis to cases with two fluid–fluid interfaces in the planar system and a similar picture resulted. In cases of large corrugations, perturbation techniques as mentioned above are no longer applicable. Pozrikidis (1988) extended Wang's problem to large corrugations by solving the two-dimensional creeping flow problem numerically on a periodic domain using a boundary integral method.

Despite the work cited on base flows, linear or nonlinear stability issues associated with flows in a corrugated configuration, especially interfacial problems, have until recently been explored only in a preliminary manner. In the case of no flow, Gauglitz & Radke (1990) employed an analysis (1988) that kept the full nonlinear circumferential component of capillarity in an otherwise linear analysis. They examined how constrictions affect the foam formation in gas–liquid displacements for the case where the tube radius varies slowly in the axial direction. They showed that the time needed to snap a collar off strongly depends on the neck radius of the constriction and that the length of the constriction is not crucial to the instability. A similar conclusion was also drawn by Ransokoff, Gauglitz & Radke (1987) and Ratulowski & Chang (1989) who analysed the case when constrictions have varied cross-sections.

In the presence of a base flow, Kelly (1967) first studied the inviscid linear stability of a stationary wave without surface tension that is periodic in space and time in the base state. He derived a resonance condition in which the disturbances can excite an instability. Tougou (1978) investigated the stability of a viscous film flowing down an inclined uneven wall in the presence of surface tension. To leading order in a shallow thickness parameter $\varepsilon$ defined as the ratio of the mean film thickness to the wall's wavelength, the linear stability of the base flow is identical to that for the plane wall case. The long-time, weakly nonlinear interfacial evolution as governed by the Kuramoto–Sivashinsky (KS) equation, however, is no longer spatially periodic owing to the non-parallel base flow.

Finally, Kouris & Tsamopoulos (2000, 2001 hereinafter referred to as KT1 and KT2) use a vorticity formulation, a time-dependent transformation into a coordinate system where both the wall and the interface are time-invariant constant coordinate surfaces and a pseudospectral method to solve numerically for the flow pattern and examine the stability of a core–annular flow in a sinusoidally varying tube. In the former work, the authors restrict themselves to disturbances that are long compared with the maximum tube radius and in both works, they are motivated by application to trickle bed reactors where the tension is, in general, not large and the dominant mechanism of instability is typically viscous stratification. Capillary numbers $Ca$, defined as the product of the core fluid viscosity and the characteristic velocity divided by the interfacial tension, are of order 0.1 or larger, Reynolds numbers $Re$ are not small and, particularly in KT2, the viscosity of the annulus fluid is much smaller than that of the core. Their results thus often involve the inertia of the film.

Our goal in this study is to develop a systematic approach to investigate the effect of pore corrugation on the instability of a core–annular film flow in the strong surface tension limit and to see how a non-trivial base flow interacts with a disturbance to determine the system's stability. The existing works based on PCAF theory can be regarded as a limiting case of our analysis.

Clearly, we would like to examine the effect of wall corrugation in general. However, owing to its complexity, we make a number of simplifications to idealize the geometry and thus make the problem analytically tractable. First, we derive the equations for

the base flow and its linear stability for a corrugation of arbitrary structure, absent sharp gradients, with amplitude $\sigma\varepsilon$, but we carry out our detailed calculations for a sinusoidal shaped corrugation. Here, as before, the parameter $\varepsilon$ is the ratio of the mean annulus thickness to the mean core radius. Small $\varepsilon$ corresponds to the thin-film limit. The corrugation parameter $\sigma$ is measured with respect to the film thickness and can be $O(1)$ in general. Of course, $\sigma = 0$ should reduce to the straight tube case. Thus, $\sigma\varepsilon$ is small relative to the macroscopic geometry of the tube. However, when $\varepsilon \ll 1$ and $\sigma \sim O(1)$, even though $\sigma\varepsilon$ is small with respect to the core radius, it is still comparable to the film thickness; in that case, the film equations are difficult to handle owing to the quadratic terms arising when applying the boundary conditions at the corrugated wall. If, on the other hand, the corrugation is also small compared with the film thickness (i.e. $\sigma \ll 1$), then we can, at the cost of an additional small parameter, linearize the corrugation and simplify the formulation without abandoning our objective. Thus, by means of perturbation techniques, one can expect the steady base flow to be a superposition of a parallel flow in the cylindrical tube and a correction for non-parallel fluid motion arising from the corrugation, to leading order in the small parameter. We can then perform a stability analysis, order-by-order in the perturbation parameter with the corresponding base flow. We extend this analysis into the weakly nonlinear regime in the companion paper (Wei & Rumschitzki 2002).

In contrast to KT1 and KT2, we examine the strong tension $Ca \sim \varepsilon^2$, $\varepsilon \ll 1$, slow flow $Re \leqslant O(1)$ regime where surface tension is the prime player, and focus on comparable viscosities or a thicker annulus fluid. As a result, direct numerical comparison between our asymptotic results and their numerics is not possible. Nevertheless, there are a number of parameter dependences that arise from their calculations that appear to extend to our parameter regime, and our analytic asymptotic equations below may shed some light on their origins. Moreover, both they and we find that corrugation makes a core–annular flow less stable.

## 2. Governing equations and boundary conditions

Two immiscible, viscous, incompressible fluids are flowing axisymmetrically without gravity in a core–annular arrangement in a tube of radius $R_2(z)$ that varies in the axial direction with slight corrugation. See figure 1. The interface is given by $r = S(z,t)$. The core region, defined by $0 \leqslant r \leqslant S(z,t)$, is occupied by fluid 1 and the annulus, $S(z,t) \leqslant r \leqslant R_2(z)$, is filled by fluid 2. Since the flow fields are assumed to be axisymmetric, they only have velocity components $(u, 0, w)$ in terms of the cylindrical polar coordinates $(r, \theta, z)$. We non-dimensionalize the velocity, pressure, length scales, and time with the characteristic quantities $W_0$, $\rho W_0^2$, $R_0$ and $R_0/W_0$, respectively, where $W_0$ is the axial velocity at the central line $r = 0$ in the uncorrugated base flow (for a gas core one would use the unperturbed interfacial velocity), $\rho$ is the density of the fluids taken for now to be equal, and $R_0$ is the mean radius of the core. Then, the governing equations are

$$w_t + uw_r + ww_z = -p_z + \frac{1}{Re_i}\nabla^2 w, \tag{2.1a}$$

$$u_t + uu_r + wu_z = -p_r + \frac{1}{Re_i}\left(\nabla^2 u - \frac{u}{r^2}\right), \tag{2.1b}$$

$$\frac{1}{r}(ru)_r + w_z = 0, \tag{2.1c}$$

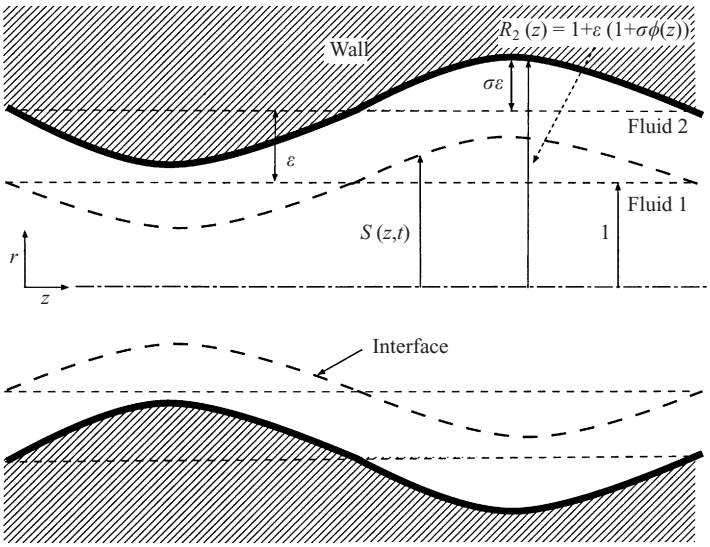


FIGURE 1. The flow geometry of a core–annular flow in a corrugated tube.

where subscripts represent partial derivatives,

$$\nabla^2 = \frac{\partial^2}{\partial r^2} + \frac{1}{r}\frac{\partial}{\partial r} + \frac{\partial^2}{\partial z^2},$$

$i = 1, 2$ denotes the core and the annulus, respectively, and the Reynolds number is given by $Re_i = \rho W_0 R_0/\mu_i$, $\mu_i$ being the viscosity of fluid $i$, $i = 1, 2$. We use the capital letters, $U$, $W$ and $P$ to denote the core's radial and axial velocities and pressure and the lower case letter $u$, $w$ and $p$ for the corresponding film quantities. Clearly, $Re_2 = Re_1/m$, in which $m = \mu_2/\mu_1$ is the viscosity ratio of the annulus to the core.

The following boundary conditions should be used: the velocities vanish at the wall,

$$w = 0, \quad u = 0 \quad \text{at} \quad r = R_2(z). \tag{2.2a}$$

Define the jump notation $[\bullet] = (\bullet)_1 - (\bullet)_2$. The velocities are continuous across the interface,

$$[w] = 0, \quad [u] = 0 \quad \text{at} \quad r = S(z,t). \tag{2.2b}$$

The tangential stress and normal stress balances at the interface $r = S(z,t)$ are

$$\left[\frac{1}{Re}(u_z + w_r)(1 - S_z^2) + \frac{2}{Re}u_r S_z - \frac{2}{Re}w_z S_z\right] = 0, \tag{2.2c}$$

$$-\left[p - \frac{2}{Re}u_r - \left(-p + \frac{2}{Re}w_z\right)S_z + \frac{2}{Re}(u_z + w_r)S_z\right] = \frac{J}{Re_1^2}\left(S_{zz} - \frac{1}{S}(1 + S_z^2)\right)(1 + S_z^2)^{-3/2}, \tag{2.2d}$$

where $J = \sigma_s R_0/\rho v_1^2$ is the surface tension parameter used by Chandrasekhar (1968) and $\sigma_s$ is the interfacial tension. The kinematic condition, which determines the shape of the interface, is

$$u = S_t + wS_z \quad \text{at} \quad r = S(z,t). \tag{2.2e}$$

Finally, the core flow field must be bounded at the central line, i.e.

$$W, U \text{ bounded as } r \to 0. \tag{2.2f}$$

## 3. Base flow

### 3.1. *Scalings*

Consider the above arrangement, in the presence of surface tension and viscosity stratification, but neglecting density differences and gravity. To zeroth order in the corrugation parameter $\sigma$ (i.e. no corrugation), the flow patterns in both fluids are parallel, i.e.

$$\bar{\bar{w}} = \frac{a^2 - r^2}{a^2 + m - 1}, \quad \overline{\overline{W}} = 1 - \frac{mr^2}{a^2 + m - 1}, \tag{3.1a,b}$$

where $a = 1 + \varepsilon$ is the non-dimensional (mean) radius of the tube and $\varepsilon$ is the ratio of the (mean, when $\sigma \neq 0$) undisturbed film thickness to the (mean) core radius. The thin-film limit requires $\varepsilon \ll 1$. Since the film variables vary over a radial distance $\varepsilon$, we introduce a stretched film variable $y := 1 - (r - 1)/\varepsilon$. Here, $y = 0$, 1 corresponds to $r = 1 + \varepsilon$, 1, i.e. the (average) position of the wall and the fluid–fluid interface, respectively. Then, since $m = O(1) \gg \varepsilon$, the $\sigma = 0$ velocity profile of the annular layer is a linear shear flow to order $\varepsilon$: $\bar{\bar{w}} = (2\varepsilon/m)y + O(\varepsilon^2)$. The core flow is still parabolic, i.e. $\overline{\overline{W}} = 1 - r^2 + (2\varepsilon/m)r^2 + O(\varepsilon^2)$. The interface is the perfectly cylindrical surface $r = 1$. The thin-film, unlike the core, can only support an axial correction to the driving pressure gradient in response to a corrugation and it transmits this variation to the core via an interfacial deflection. Let us begin by examining the scalings that govern the perturbed base flow.

The corrugated wall is given by $R_2(z) = 1 + \varepsilon(1 + \sigma\phi(z))$ or $y = -\sigma\phi(z)$, where $\phi(z)$ is a prescribed order-one function of $z$, the corrugation factor $\sigma$ is assumed to be small compared with 1, and $\sigma = 0$ gives the uncorrugated system. Let the perturbed (due to $\sigma \neq 0$) quantities ($\bar{w}'$, $\bar{u}'$, $\bar{p}'$) and ($\overline{W}'$, $\overline{U}'$, $\bar{P}'$) correspond to the film and core, respectively. We represent the steady interface, perturbed by the wall's corrugation, by $S_b(z) = 1 + \bar{\delta}\eta(z)$, where $\eta(z)$ is an unknown order-one function. We shall seek scalings for the above dynamic quantities and for the perturbed interface ($\bar{\delta}$) in terms of $\varepsilon$ and $\sigma$.

The introduction of the thin-film variable $y$ makes the thin-film limit ($\varepsilon \to 0$) explicit. It also separates the radial scale of the film from the axial scale and from both scales in the core. As such, radial derivatives in the film are large, i.e. $\partial/\partial r = -(1/\varepsilon)(\partial/\partial y)$. To find the appropriate scalings, we follow the procedures used by Hammond (1983) or Papageorgiou, Maldarelli & Rumschitzki (1990). The scalings follow from the fact that the thin annulus can support only a lubrication flow. Let us begin by considering the no-slip condition for the axial velocity at the wall ($y = -\sigma\phi(z)$) and the Taylor expansion about $y = 0$. This gives $\bar{w}' \sim \sigma\varepsilon/m$. Continuity gives $\bar{u}' \sim \varepsilon\bar{w}' \sim \sigma\varepsilon^2/m$. Meanwhile, the steady-state kinematic condition gives $\bar{\delta} \sim \bar{u}/\bar{\bar{w}} \sim \sigma\varepsilon$. This deflection causes a perturbed pressure across the interface. In general, thin-film shear flows develop dominant pressures that drive lubrication-layer flows. Therefore, the film's perturbed pressure dominates the normal stresses and balances the surface tension terms. We can estimate it as $\bar{p}' \sim J\bar{\delta}/Re_1^2 \sim J\varepsilon\sigma/Re_1^2$. It follows from (2.1*a*) that the perturbed axial velocity in the film scales as $\bar{w}' \sim J\bar{\delta}\varepsilon^2/m\,Re_1$ from the film's lubrication equations. Equating these orderings with those derived from the no-slip condition gives $J/Re_1 \sim 1/\varepsilon^2$. This is the scaling relation necessary in order to obtain

the non-trivial base state and the corresponding stability analysis. Let us turn to the core scalings. So as to over-determine neither the film nor the core problem, there needs to be a balance between core and film quantities in either the tangential stress condition or the continuity of axial velocity at the interface. The former case leads to a trivial solution to leading order in the core. Thus, the continuity of the axial velocities at the interface dictates the $\overline{W}'$ scale. The lack of $(r\text{–}z)$-scale separation in the core then determines that $\overline{W}'$ and $\overline{U}'$ are both of order $\sigma\varepsilon/m$ and $\bar{P}' \sim \sigma\varepsilon/m\,Re_1$. Based on such scalings, the leading-order tangential stress balance is dominated by the film flow. As we shall see, the corrugated base state is film-determined as in Hammond and the core slaves the film.

There are two different consistent situations here. One considers slow fluid motions and large surface tension, i.e. $Re_1 \sim \varepsilon$ and $J \sim 1/\varepsilon$, or order-one flows and very large surface tensions $Re_1 = O(1)$ and $J \sim 1/\varepsilon^2$ corresponding to moderate fluid motions. In the former case, the core's inertia is negligible and the core flow is governed by the Stokes equations. In the latter, the core's inertia enters in a perturbative manner and its flow pattern is expected to be expressible in terms of Kummer's hypergeometric function. However, as previously mentioned, owing to the core-slaving of the film, these cases differ in their core flow patterns but have identical film flows. Accordingly, the surface tension number $J$ and Reynolds number always appear in the film solution as $J/Re_1$, i.e. together and not individually. Thus, since it is the film flow that dictates the system's stability and both cases yield the same film flow, we choose to concentrate in the present work mainly on the creeping flows corresponding to the former case.

For $Re_1 \sim \varepsilon$, $J \sim 1/\varepsilon$, we posit regular perturbation expansions and substitute into the governing equations and boundary conditions to derive the leading-order steady corrugated flow problem.

### 3.2. *The leading-order base flow*

Following the scales outlined, the film flow has the following asymptotic expansions:

$$w = \bar{\bar{w}} + \sigma\varepsilon\bar{w} + O(\sigma^2\varepsilon, \sigma\varepsilon^2), \tag{3.2a}$$

$$u = \sigma\varepsilon^2\bar{u} + O(\varepsilon^2\sigma^2, \varepsilon^3\sigma), \tag{3.2b}$$

$$p = \bar{\bar{p}} + \frac{\sigma}{\varepsilon^2}\bar{p} + O\left(\frac{\sigma^2}{\varepsilon^2}, \frac{\sigma}{\varepsilon}\right). \tag{3.2c}$$

For the core,

$$W = \overline{\overline{W}} + \sigma\varepsilon\overline{W} + O(\varepsilon\sigma^2, \varepsilon^2\sigma), \tag{3.2d}$$

$$U = \sigma\varepsilon\overline{U} + O(\varepsilon\sigma^2, \varepsilon^2\sigma), \tag{3.2e}$$

$$P = \bar{\bar{P}} + \sigma\bar{P} + O(\sigma^2, \varepsilon\sigma), \tag{3.2f}$$

where a double overbar denotes the uncorrugated base state which is a two-fluid Poiseuille flow and has a uniform pressure gradient in each region, and a single overbar denotes the corrugated base state correction. Substituting (3.1*a*), (3.1*b*) and (3.2*a*)–(3.2*f*) into the governing equations (2.1*a*)–(2.1*c*) and boundary conditions (2.2*a*)–(2.2*f*) expanded around the uncorrugated state ($\sigma = 0$), eliminating the zeroth-order of corrugation and letting $Re_1 = \varepsilon\lambda$ and $J = J_0/\varepsilon$, where $\lambda$ and $J_0$ are $O(1)$, gives the leading-order equations in $\sigma$ and $\varepsilon$:

For the film,

$$0 = -\bar{p}_z + \frac{m}{\lambda}\frac{\partial^2 \bar{w}}{\partial y^2}, \tag{3.3a}$$

$$0 = \bar{p}_y, \tag{3.3b}$$

$$-\frac{\partial \bar{u}}{\partial y} + \frac{\partial \bar{w}}{\partial z} = 0. \tag{3.3c}$$

For the core,

$$0 = -\bar{P}_z + \frac{1}{\lambda}\nabla^2 \overline{W}, \tag{3.3d}$$

$$0 = -\bar{P}_r + \frac{1}{\lambda}\nabla^2 \left(\overline{U} - \frac{\overline{U}}{r^2}\right), \tag{3.3e}$$

$$\frac{1}{r}\frac{\partial}{\partial r}(r\overline{U}) + \frac{\partial}{\partial z}\overline{W} = 0. \tag{3.3f}$$

The boundary conditions become the following:
At $y = 0$ (the $\sigma = 0$ wall),

$$\bar{w} = \frac{2\phi}{m}, \quad \bar{u} = 0. \tag{3.4a}$$

At $r = 1$ or $y = 1$ (the $\sigma = 0$ interface), the velocities are continuous:

$$\overline{W} - 2\eta = \bar{w} - \frac{2}{m}\eta, \quad \overline{U} = 0. \tag{3.4b}$$

Tangential stress:
$$m\frac{\partial \bar{w}}{\partial y} = 0, \tag{3.4c}$$

Normal stress:
$$\bar{p} = \frac{J_0}{\lambda^2}(\eta_{zz} + \eta), \tag{3.4d}$$

Kinematic condition:
$$\bar{u} = \frac{2}{m}\eta_z, \tag{3.4e}$$

At the centreline,

$$\text{as } r \to 0, \overline{W} \text{ and } \overline{U} \text{ are bounded.} \tag{3.4f}$$

The solution of (3.3), subject to (3.4*a*) and (3.4*c*), is the film's velocity profile in terms of the prescribed wall function $\phi$ and the unkown interface function $\eta$:

$$\bar{w}(y,z) = \frac{\lambda}{m}\bar{p}_z(\tfrac{1}{2}y^2 - y) + \frac{2}{m}\phi(z), \tag{3.5a}$$

$$\bar{u}(y,z) = \frac{\lambda}{m}\bar{p}_{zz}(\tfrac{1}{6}y^3 - \tfrac{1}{2}y^2) + \frac{2}{m}\phi_z(z)y. \tag{3.5b}$$

By substituting the film's velocity and pressure into the static kinematic condition (3.4*e*) and integrating once d$z$, we obtain an equation for the leading-order static interfacial deflection

$$\frac{J_0}{3m\lambda}(\eta_{zzz} + \eta_z) + \frac{2}{m}\eta = \frac{2}{m}\phi. \tag{3.6}$$

We retain the common factor $m$ for our discussion of the physical meanings of

the terms in (3.6) later in the stability analysis. Note that, when deriving (3.6), an additional constant of integration $2c/m$ appears. A redefinition of

$$\eta \to \eta + 2c/m \tag{3.7}$$

absorbs this arbitrary constant, which has the effect of changing the $\sigma = 0$ film flow rate.

The perturbation pressure gradient drives a perturbed base flow via the interfacial deflection. Since the fluids are viscous, a shear stress in the core fluid balances this pressure gradient. We expect the deflection $\eta$ of the interface to be independent of the viscosity ratio $m$, since both the normal and the tangential components of the stress conditions are film-dominated, i.e. contain only film variables to leading order. Observe also from (3.6) that the interface will be out of phase with the wall; shear tends to align the interface and the wall, whereas the interfacial tension (in $J_0$) introduces a phase-shift motion. As expected, the higher the interfacial tension, the higher the interface–wall phase shift.

From the solution of (3.6) for the shape function $\eta$ of the interface, we can obtain the complete solution for the film by plugging into (3.5$a$) and (3.5$b$). The solution to (3.6) should be a linear combination of a homogeneous and a particular solution. However, since the wavenumber of the homogeneous solution is complex, we set its coefficients to zero because otherwise the homogeneous solution would lead to an unbounded interface as $|z| \to \infty$. We therefore retain only the particular solution. If the wall function $\phi$ is periodic to the leading order in the corrugated base flow, the interface should also be periodic with the same periodicity as the wall. The trial solution $\eta = c_1 \cos(kz) + c_2 \sin(kz)$, or $(\phi, \eta) = (\hat{\phi},\ \hat{\eta}) \exp(\mathrm{i}kz) + (\hat{\phi}^*,\ \hat{\eta}^*) \exp(-\mathrm{i}kz)$ yields

$$\hat{\eta} = \frac{1}{1 + \dfrac{J_0}{6\lambda} \mathrm{i}k(1-k^2)} \hat{\phi}. \tag{3.8}$$

The film base velocities $w_0 = \bar{\bar{w}} + \bar{w}$ and $u_0 = \bar{u}$ follow from (3.4$d$) and (3.5). For the core flow at the leading order of the corrugation, define a stream function $\overline{\Psi}$ such that

$$\overline{W} = \frac{1}{r}\frac{\partial \overline{\Psi}}{\partial r}, \quad \overline{U} = -\frac{1}{r}\frac{\partial \overline{\Psi}}{\partial z}. \tag{3.9}$$

$\overline{\Psi}$ satisfies the creeping flow equations

$$\mathrm{E}^2\mathrm{E}^2\overline{\Psi} = 0, \tag{3.10}$$

where

$$\mathrm{E}^2 = \frac{\partial^2}{\partial r^2} - \frac{1}{r}\frac{\partial}{\partial r} + \frac{\partial^2}{\partial z^2},$$

and is subject to (3.4$b$) and (3.4$f$).

Since $\eta$ is already known in terms of $\phi$, we can solve the core flow for $\overline{\Psi} = \hat{\Psi}(r) \exp(\mathrm{i}kz)$ to obtain

$$\hat{\Psi}(r) = ArI_1(kr) + Br^2 I_0(kr), \tag{3.11}$$

where $I_i(r)$ is the modified Bessel functions of order $i$ and

$$A = \frac{1}{(2-k)I_0(k) + kI_1(k)} \left( -\frac{I_0(k)}{I_1(k)} \left( \left( 2 + \frac{1}{m} \right) \hat{\eta} - \frac{1}{m}\hat{\phi} \right) \right), \tag{3.12$a$}$$

$$B = \frac{1}{(2-k)I_0(k)+kI_1(k)}\left(\left(2+\frac{1}{m}\right)\hat{\eta}-\frac{1}{m}\hat{\phi}\right). \tag{3.12b}$$

The core velocities follow from (3.9). The base flow is film-determined and the core slaves the film. For a moderate flow $Re_1 \sim O(1)$, $J \sim 1/\varepsilon^2$, the pertubed pressures $\bar{p}' \sim \sigma/\varepsilon$ rather than $\sim \sigma/\varepsilon^2$ and $\bar{P}' \sim \sigma\varepsilon$ rather than $\sim \sigma$ in the film and core, respectively, and the perturbed velocities retain the same orderings as earlier. As a result, the formulation of the film problem remains unchanged, whereas that of the core flow will be altered. Let $J = J_0/\varepsilon^2$ and $Re_1 = \lambda$. The core equations are continuity (3.3*f*) and

$$-2r\overline{U}+(1-r^2)\overline{W}_z = -\bar{P}_z+\frac{1}{\lambda}\nabla^2\overline{W}, \quad (1-r^2)\overline{U}_z = -\bar{P}_r+\frac{1}{\lambda}\left(\nabla^2\overline{U}-\frac{\overline{U}}{r^2}\right). \tag{3.13a,b}$$

We again introduce the streamfunction used earlier to eliminate $\bar{P}$ to obtain

$$(1-r^2)\frac{\partial}{\partial z}(\mathrm{E}^2\overline{\Psi}) = \mathrm{E}^2\mathrm{E}^2\overline{\Psi}. \tag{3.14}$$

Following Papageorgiou *et al.* (1990), we can solve the core in terms of Kummer's confluent hypergeometric function $M(b,2,2ar^2)$ (Abramowitz & Stegun 1972), where $a = \frac{1}{2}(k\lambda)^{1/2}\mathrm{e}^{-\mathrm{i}\pi/4}$ and $b = 1+k^2/8a-\frac{1}{2}a$. The solution for the Fourier transform of the core's streamfunction is

$$\hat{\Psi}(r) = A_1(k)rI_1(kr)+B_1(k)rN_1(kr), \tag{3.15}$$

$$A_1(k) = \frac{((2+1/m)\hat{\eta}-\hat{\phi}/m)N_1(k)}{k[N_1(k)I_0(k)-N_0(k)I_1(k)]}, \quad B_1(k) = -\frac{((2+1/m)\hat{\eta}-\hat{\phi}/m)I_1(k)}{k[N_1(k)I_0(k)-N_0(k)I_1(k)]},$$

$$N_j(kr) = \int_0^r [I_j(k)K_1(kt)-I_j(kt)K_1(kt)]t^2\exp(-at^2)M(b,2,2at^2)\,\mathrm{d}t, \quad (j=0,1).$$

### 3.3. *The leading-order base flow: results*

Since we consider only the particular solution, the base flow in the corrugated configuration exhibits the same periodicity as the wall. Because the film is very thin, its inertia is negligible (this is a consequence of its lubrication flow) and the corrugation of the wall propagates into the flow via the viscous shear and the perturbation pressure. Typical streamlines in the film are shown in figure 2. The streamlines are almost in phase with the wall (no-slip) near the wall and become increasingly out of phase with increasing $y$. In addition, the magnitude of the spatial oscillation of the streamlines decreases with increasing distance from the wall in the film owing to the interface's resistance to being corrugated. KT1 and KT2, also calculate steady interfacial shapes. They find for low $Re$ and low surface tension ($J/(mRe) \ll 1$ in our notation), the interface exhibits the fore–aft symmetry of Stokes flow, in agreement ($\eta = \phi$) with our equation (3.6). Equation (3.6) also dictates that this symmetry is broken by raising $J/(mRe)$. Despite the disparity in parameter values between these studies, this seems to explain Kouris & Tsamopoulos' loss of symmetry by raising their Reynolds number, inverse Weber number $W$, or lowering their viscosity ratio $\mu$ (our $J/(mRe)$ is equal to their $ReW/(\Lambda\mu)$, modulo an $O(1)$ adjustment owing to a different choice of characteristic velocity). They find recirculation in the film in the tube crests for large $\varepsilon$ and high $Re$, which are beyond the scope of our theory.

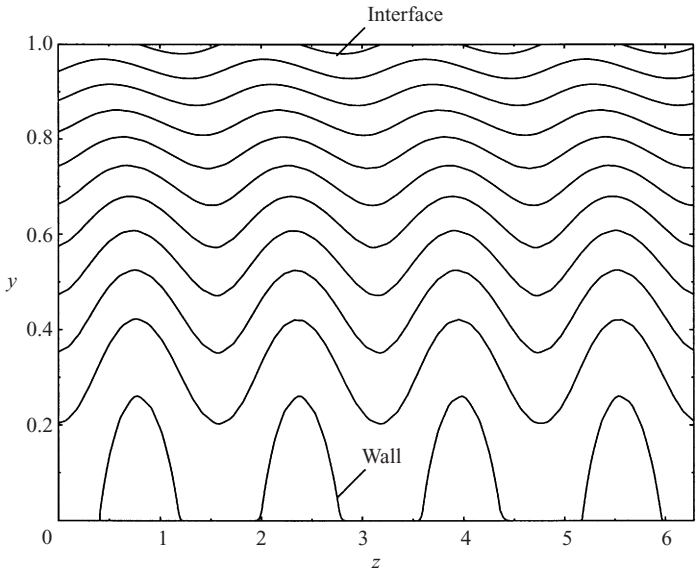


FIGURE 2. A typical streamline of the base film flow. Flow is to the right. $J_0/\lambda = 1.0$, $m = 1.0$, $k = 4.0$, $\sigma = 0.2$.

The amplitude $Amp$ of $\eta$ and the interface–wall phase shift $\theta$ characterize the base flow:

$$Amp = \frac{1}{\sqrt{1 + \left[\frac{J_0}{6\lambda}k(1-k^2)\right]^2}}, \tag{3.16}$$

$$\theta = \tan^{-1}\left(-\frac{J_0}{6\lambda}k(1-k^2)\right). \tag{3.17}$$

Figures 3($a$) and 3($b$) show how $Amp$ and $\theta$ depend on the wavenumber $k$ of the wall. We also compare these results with Wang's analysis of a film of a single viscous fluid flowing down a wavy inclined plate in the thin-film limit. For zero interfacial tension, $\hat{\eta} = \hat{\phi}$ and the interface and the wall remain in phase and of equal amplitude for all $k$. For infinite interfacial tension, $\hat{\eta} = 0$, and the interface is $r = 1$ for all $k$. For finite tension, the interfacial deflection/deformation decreases as $k$ increases; capillarity resists short-wave corrugations.

The phase shift reflects the relative effect of capillarity and shear. If (3.6) contained only a shear flow contribution, the interface would be in phase with the wall. Derivatives from the capillary terms induce a phase shift; shorter waves (large $k$) have a larger phase shift. Short axial waves do not see the circumferential curvature and thus reduce to the planar result.

In the absence of capillarity, $\eta = \phi$. An in-phase and equal-amplitude wall–interface configuration means that the film flow is locally parallel. If $\phi$ and $\eta$ are periodic and in phase, there should be no net additional flow rate due to the interfacial corrugation. Mathematically, consider the film's flow rate calculated via (3.7) and evaluated at a node of $\phi(z)$. Requiring the corrugation to leave the flow rate unchanged to leading order yields an equation of the form $f(\eta, \eta_z, \eta_{zzz}) = 0$. If $\phi$ and $\eta$ are periodic and in phase, this equation has no unknowns for a fixed $k$ and cannot, in general, be

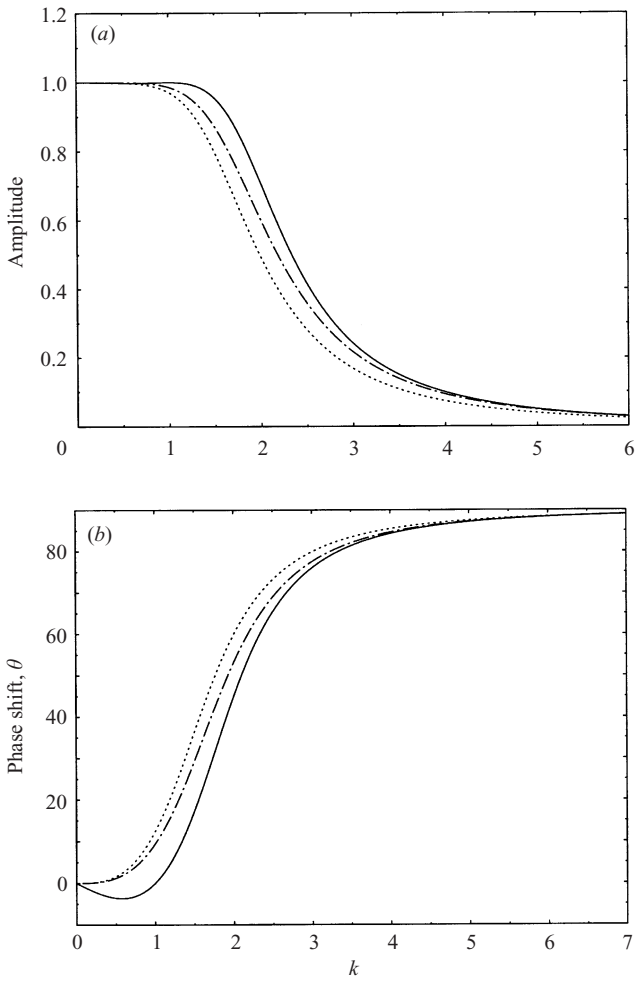


FIGURE 3. (*a*) The interfacial amplitude *vs.* $k$. (*b*) The phase shift between the interface and the wall *vs.* $k$. $J_0/\lambda = 1.0$, $m = 1.0$. ——, present case; – · –, planar case; · · ·, Wang.

satisfied. On the other hand, if $\eta$ and $\phi$ are periodic and of the same form but with a phase angle $\theta$ between them, then $f(\eta, \eta_z, \eta_{zzz}; \theta) = 0$ allows a solution where different phase angles $\theta$ correspond to different induced flow rate corrections. Finally, as for the shape of figure 3(*b*), consider a simple $\sin(kz)$ profile. For short waves, the longitudinal contribution, which goes as $k^3\cos(kz)$, dominates the circumferential contribution of $-k\cos(kz)$ to give the planar result. However, for long waves, the latter dominates and leads to a negative phase shift. The magnitude of this phase shift increases as the interfacial tension increases.

The special case $k = 1$ results in the circumferential and longitudinal curvature contributions balancing and thus in $\eta = \phi$. Thus, the interface shape again exactly follows the wall and the flow pattern is locally parallel. As we shall see, the corresponding linear stability for this particular case is the same as that for the uncorrugated case to leading order in $\varepsilon$.

Since this discussion focuses exclusively on the film, it applies equally well to the case of $O(1)$ Reynolds number and very high interfacial tension $O(1/\varepsilon^2)$, where

the capillary force again appears as $J/Re_1 \sim O(1/\varepsilon^2)$. As we shall see below, the corresponding linear stability analysis will also not rely on details of the core's dynamics and both cases will be governed by the same interfacial evolution equation. Thus, the cases differ only in the core's dynamics.

The above analysis is based on the scaling $J/Re_1 = 1/Ca \sim 1/\varepsilon^2$, where the capillary number $Ca = \mu_1 \overline{\overline{W}}(r = 0)/\sigma_s = Ca_0\varepsilon^2$, i.e. strong surface tension. As we shall see, the linear stability equation corresponding to small $Ca_0$ is similar (to the leading order in $\varepsilon$) to a linearized version of Hammond's (1983) problem with no base flow. If $\varepsilon^2 J/Re_1 \gg 1$, then the surface tension will dominate ($p_z$ will dominate $w_{rr}$ in the equation of motion), and to leading order in $\sigma$, the base flow interface will simply be cylindrical and the wavenumber of a disturbance $\alpha = 1$ will be a neutral mode. If $\varepsilon \ll \varepsilon^2 J/Re_1 \ll 1$, capillarity will not affect the interface's shape ($\eta = \phi$) to leading order ($w_{rr}$ will dominate the equation of motion). These results agree with simply taking the corresponding limit of (3.6).

## 4. Linear stability

### 4.1. *Scalings*

With the asymptotic, steady base flows derived above, we now begin the corresponding asymptotic linear stability analysis. Let us introduce an infinitesimal, axisymmetric disturbance of size $\delta(\delta \ll \sigma, \varepsilon)$ at the steady interface in such a way that $S(z,t) = S_b(z) + \delta\xi(z,t)$, where $S_b(z)$ is the interface of the corrugated base state and $\xi(z,t)$ is an unknown order-one function responsible for the disturbance. In analogy to the procedure used in treating the base flows, we first estimate the scalings of the disturbed quantities before formulating the perturbation scheme. If $(w', u', p')$ and $(W', U', P')$ represent the disturbed quantities for the film and the core, respectively, then following Georgiou *et al.* (1992), we can estimate the scalings of these quantities in the case of $Re_1 \sim \varepsilon$ and $J \sim 1/\varepsilon$ from the scaling relations used in the base flows and from the governing equations and boundary conditions. From the normal stress condition, $p' \sim \delta/\varepsilon^3$. Balancing $w'$ with $p'$ in the lubrication equations in the film gives $w' \sim \delta$, and $u' \sim \varepsilon\delta$ follows by continuity. By reasoning similar to that in the base flow for the core, both $W'$ and $U'$ are order $\delta$, and $P'$ is order $\delta/\varepsilon$. By plugging the appropriate asymptotic expansions into the governing equations and boundary conditions and extracting the corrugated base flow's contribution, we derive a set of equations that govern the system's stability to leading order in $\delta$.

### 4.2. *Formulation of the linear stability*

Following the above scalings, and redefining the primed quantities to make their scalings explicit, we define the following asymptotic expansion for the disturbed flow quantities:

For the film (4.1*a–c*) and the core (4.1*d–f*),

$$w = \bar{w} + \delta w', \quad u = \bar{u} + \varepsilon\delta u', \quad p = \bar{p} + \frac{\delta}{\varepsilon^3}p', \tag{4.1a–c}$$

$$W = \overline{W} + \delta W', \quad U = \overline{U} + \delta U', \quad P = \bar{P} + \frac{\delta}{\varepsilon}P', \tag{4.1d–f}$$

where the bar quantities denote the base flow quantities, which have non-trivial $\sigma$ and $\varepsilon$ expansions. If the asymptotic series converge, full knowledge of this base state to all orders in $\sigma$ and $\varepsilon$ provides an exact solution of the nonlinear, steady-state Navier–Stokes equation subject to the corrugated boundary's conditions. We

have solved only the base flow asymptotically and have thus far only determined its leading-order contributions explicitly. However, when substituting (4.1) into (2.1) and (2.2), we use the fact that the full steady-state solution satisfies the steady equations and boundary conditions exactly and its truncated solutions satisfy these equations/conditions exactly up to the order of truncation; this will allow us to retain only terms of $O(\delta)$ and lower. The coefficients will only contain explicit contributions from the leading-order corrugated base flow. Thus, details of the higher-order base state solutions are not required.

The film's (4.2*a–c*) and core's (4.2*d–f*) governing equations become

$$0 = -p'_z + \frac{m}{\lambda} w'_{yy}, \quad 0 = p'_y, \quad -u'_y + w'_z = 0, \tag{4.2a–c}$$

$$0 = -P'_z + \frac{1}{\lambda}\nabla^2 W', \quad 0 = P'_r + \frac{1}{\lambda}\left(\nabla^2 U' - \frac{U'}{r^2}\right), \quad \frac{1}{r}(rU')_r + W'_z = 0, \tag{4.2d–f}$$

subject to the following boundary conditions. On the wall:

$$y = -\sigma\phi, \quad w' = 0, \quad u' = 0. \tag{4.3a}$$

At the interface, we expand around the base state interface $S_b(z)$ and use the base flow to eliminate terms. The resulting leading terms in $\varepsilon$ and $\delta$ are: the continuity of the velocity components at the interface contributes the following $O(\delta)$ terms:

$$-\xi\left(\frac{2}{m} + \sigma\bar{w}^{(1)}_{\gamma}\right)_{y=1} + w'(y = 1 - \sigma\eta) = -2\xi + W'(r = 1) + O(\sigma\varepsilon),$$

$$U'(r = 1) = O(\varepsilon). \tag{4.3b}$$

The tangential stress leads with $O(\delta/\varepsilon)$ and is dominated by the film:

$$-w'_y(y = 1 - \sigma\eta) + \sigma\xi\bar{w}^{(1)}_{yy}(y = 1) = O(\varepsilon). \tag{4.3c}$$

Note that the base film flow causes an $O(\delta\sigma/\varepsilon)$ perturbation in the tangential stress at the interface due to the corrugation. In order to bring this effect of corrugation into the leading order and at the same time to avoid any coupling with the core (i.e. $O(\delta\sigma/\varepsilon) \gg O(\delta)$), we also assume $\sigma \gg \varepsilon$.

Here again, the leading $O(\delta)$ normal stress balance has only a film contribution:

$$\text{at } y = 1 - \sigma\eta, \quad p' = \frac{J_0}{\lambda^2}(\xi_{zz} + \xi) + O(\sigma\varepsilon). \tag{4.3d}$$

Note that unlike (4.3*b*) and (4.3*c*), the normal stress condition for the disturbed interface does not contain the base flow (neither its interface nor its pressure) at leading order. From the normal stress (2.2*d*), the curvature $\kappa$ can be split up as $\kappa = \kappa_b + \kappa'$, where

$$\kappa_b = \left[S_{bzz} - \frac{1}{S_b}(1 + S_{bz}^2)\right](1 + S_{bz}^2)^{-3/2}$$

represents the curvature arising from the base state's interface $S_b$, and the disturbed curvature is

$$\kappa' = \delta\left\{\xi_{zz} + \frac{\xi}{S_b^2}(1 + S_{bz}^2) - \frac{2}{S_b}S_{bz}\xi_z - \xi_z S_{bz}\left[\frac{S_{bzz}}{(1 + S_{bz}^2)} - \frac{1}{S_b}\right]\right\}(1 + S_{bz}^2)^{-3/2} + O(\delta^2).$$

The corrections to (4.3*d*) deriving from $\kappa'$ are of order $\sigma\varepsilon$ or higher and are thus not retained.

Finally, the leading order $O(\delta)$ of the kinematic condition gives

$$-\sigma\varepsilon\bar{u}_y^{(1)}(y=1)\xi+\varepsilon u'(y=1-\sigma\eta)=\xi_z+\left(\frac{2\varepsilon}{m}(1-\sigma\eta)+\sigma\varepsilon\bar{w}^{(1)}(y=1)\right)\xi_z + \left(-\frac{2}{m}\xi+w'(y=1)\right)\sigma\varepsilon\eta_z+O(\varepsilon^2). \quad (4.3e)$$

This suggests introducing a long time scale $\tau=\varepsilon t$ to eliminate $\varepsilon$ from the leading order of (4.3$e$).

At the centreline $r=0$, $W'$ and $U'$ are bounded. Solving for $w'$ and $u'$ from (4.2$a$)–(4.2$c$) gives

$$w'=\frac{\lambda}{2m}p_z'y^2+Cy+D, \quad u'=\frac{\lambda}{6m}p_{zz}'y^3+\tfrac{1}{2}C_zy^2+D_zy+E, \quad (4.4a,b)$$

where $C=-(\lambda/m)p_z'(1-\sigma\eta)+O(\sigma^2)$, $D=-(\lambda/m)p_z'\sigma\phi+O(\sigma^2)$ and $E=O(\sigma^2)$. We substitute (4.4) into (4.3$e$) to derive an asymptotic form of the film's evolution equation inclusive of corrugation. With the knowledge of the steady corrugated base flow (3.5) and the corresponding interfacial shape determined by equation (3.6), the kinematic condition (4.3$e$) yields the following leading-order interfacial evolution equation involving corrugation describing the system's linear stability:

$$\xi_\tau+\frac{2}{m}\xi_z+\frac{J_0}{3m\lambda}(\xi_{zz}+\xi)_{zz}+\sigma\left[(\eta-\phi)\left(\frac{4}{m}\xi-\frac{J_0}{m\lambda}(\xi_{zz}+\xi)_z\right)\right]_z+O(\varepsilon,\sigma^2)=0. \quad (4.5)$$

This equation consists of an $O(1)$ straight tube contribution and of a new $O(\sigma)$ term in square brackets arising from the (small) corrugation. Recall that we have assumed $\sigma\gg\varepsilon$ to bring the corrugation into the leading orders. The dependence on the corrugation is reflected by the variation of the base film's thickness $(\eta-\phi)$, which is given by the solution to (3.6). In a related problem, Coward, Papageorgiou & Smyrlis (1995) examined the weakly nonlinear stability of a core–annular flow under an oscillatory pressure gradient in a tube of uniform cross-section for small $\varepsilon$. To leading order in $\varepsilon$, they found an oscillatory contribution only to the coefficient of the weakly nonlinear term.

### 4.3. *Analysis of the linear stability*

To order $\sigma\varepsilon\delta$, the interfacial evolution equation (4.5) derived for $J\sim1/\varepsilon$, $Re_1\sim\varepsilon$ does not contain core quantities, just the wall and base flow interface functions $\phi(z)$ and $\eta(z)$. The equations for the film perturbation velocities $u'$ and $w'$ are explicit in $\phi$ and $\eta$ and are immediately determined by the solution $\xi(z,\tau)$. Calculation of $U'$ and $W'$ requires knowledge of $u'$ and $w'$. The core's dynamics slave those of the film.

For $\sigma=0$, i.e. the uncorrugated limit, (4.5) gives,

$$\xi_\tau+\frac{2}{m}\xi_z+\frac{J_0}{3m\lambda}(\xi_{zzzz}+\xi_{zz})=0. \quad (4.6)$$

This agrees with Georgiou *et al.* (1992) for $F=-1$ and $l=1$ (their notation, i.e. in the absence of gravity and density stratification). For $\sigma\neq0$, (4.5) involves the corrugated base flow's film thickness deviation $(\eta-\phi)$. In the special case of $k=1$, the film is uniform (i.e. $\eta=\phi$, no corrugation correction to this order), the flow pattern is locally parallel and the linear stability is the same as the case of $\sigma=0$ at the leading order in $\varepsilon$.

Before considering the detailed response of the system to a general disturbance,

we examine the limiting cases of very long waves and very short waves. Since the wavelength of the disturbance may be modified by its interaction with the corrugation, the dominant wavelength(s) may vary from a monochromatic disturbance during the system's evolution. Whether the wavelength of the system's response lies in one of these extreme regimes depends on the corrugation size $\sigma$, the initial wavelength $2\pi/\alpha$ of the disturbance, the wavelength $2\pi/k$ of the wall, and the time scale of interest.

(i) *Long-wave limit*. To examine the long-wave regime ($\alpha \ll 1$), we introduce the long length scale $z \sim O(1/\alpha) \gg 1$ by the new $O(1)$ variable $x = \alpha z$. It follows that $\partial/\partial z = \alpha(\partial/\partial x) \sim O(\alpha) \ll 1$. Using this new space variable and expanding (or using Yih's 1967 technique on) (4.5) in $\alpha$ gives:

$$\xi_\tau + \sigma(\eta-\phi)_z \frac{4}{m}\xi + \alpha\left[\frac{2}{m}\xi_x + \sigma(\eta-\phi)\frac{4}{m}\xi_x - \sigma(\eta-\phi)_z\frac{J_0}{m\lambda}\xi_x\right] + \alpha^2\left[\frac{J_0}{3m\lambda}\xi_{xx} - \sigma(\eta-\phi)\frac{J_0}{m\lambda}\xi_{xx}\right] + O(\sigma\alpha^3, \alpha^4) = 0. \quad (4.7a)$$

Note that the corrugation term $(\eta-\phi)_z$ still varies over the length scale $2\pi/k$ of the corrugated wall. If $\sigma \ll \alpha$, the growth rate is positive and goes to zero as $\alpha \to 0$, valid until times of $O(\sigma^{-1})$. This agrees with the normal long-wave behaviour discussed (Hickox 1971; Smith 1989; Chen & Joseph 1991) extensively in the corrugation-free case $\sigma = 0$.

For $\alpha \to 0$, (4.7*a*) becomes

$$\xi_\tau + A(z)\xi = 0, \quad (4.7b)$$

where $A(z) = \sigma(\eta-\phi)_z(4/m)$. The solution to (4.7*b*) is

$$\xi(z,\tau) = \xi_0(z)\exp(-A(z)\tau), \quad (4.7c)$$

for a step change disturbance $\xi_0(z)$ at $\tau = 0$. Since the base flow's film thickness $\sigma(\eta-\phi)_z$ can vary periodically in $z$, a local negative value can lead to growth. This contrasts with the straight-tube theory where, as $\alpha \to 0$, the Poiseuille base state does not give rise to growth. As we shall see in the eigenvalue spectrum, corrugation can excite modes other than the disturbance's.

(ii) *Short-wave limit*. This short-wave discussion holds only for $\alpha \sim O(1)$ compared with $\varepsilon$, since it is derived from (4.5). Equation (4.5) is based on lubrication in the film, which requires length scales $O(z) \gg O(r)$. Therefore, the film lubrication breaks down when $\alpha \sim \varepsilon$.

For very short waves ($1/\varepsilon \gg \alpha \gg 1$), we use a stretched variable $x = \alpha z$. Thus, $\partial/\partial z = \alpha(\partial/\partial x) \sim O(\alpha) \gg 1$ which, instead of the regular perturbation expansions in Yih's method, leads to a boundary-layer type perturbation due to the dramatic variation deriving from the highest (fourth) derivative. Then (4.5), in descending orders of $\alpha$, becomes

$$\xi_\tau + \alpha^4\left[\frac{J_0}{3m\lambda}\xi_{xxxx} - \sigma(\eta-\phi)\frac{J_0}{m\lambda}\xi_{xxxx}\right] + O(\alpha^3, \sigma\alpha^3) = 0. \quad (4.8)$$

Since $\alpha \gg k$, the corrugation is locally flat with respect to the disturbance. Therefore, the dominant effect in this limit is $O(\alpha^4)$ from the longitudinal capillarity. Its contribution is stabilizing, and the disturbance decays with the time, valid for a time scale $\tau \leqslant O(\sigma^{-1}\alpha^{-4})$. For longer times, as we shall see, higher harmonics from the corrugation interaction can cause long wavelengths to develop and thus cause the system to evolve beyond the short-wave range.

Note that viscosity stratification contributes a common factor $1/m$ to the spatial operator of the interfacial evolution equation (4.5) and simply rescales time. This means that the magnitude of the growth rate (including the corrugation correction) decreases as the film fluid becomes more viscous. (Note $J_0/(m\lambda) = \sigma/(\mu_2 W_0)$ contains only the film's viscosity.) This is because a more viscous outer fluid retards fluid motion and makes the system more dissipative.

### 4.4. *Solution methods for the film's evolution*

As noted, the inclusion of corrugation leads to a base flow that is no longer parallel (except for $k = 1$) and is non-uniform in the axial direction. This leads to a partial differential equation for its linear stability which has non-constant coefficients that vary in the axial direction. For such equations, the usual Fourier transform methods become much less useful. If we idealize the wall's variation as a sinusoidal profile, we should expect that the resulting base flow will lead to stability equations that will also be spatially periodic. We shall apply Floquet–Bloch theory to solve this partial differential equation. The basis of this method is a theorem by Floquet which asserts that the solution of a linear ordinary differential equation whose (non-constant) coefficients are periodic with a common period is the product of an exponential and a periodic function, the latter having the same period as the coefficients. In practice, if we introduce, say, a monochromatic Fourier mode $\exp(\mathrm{i}\alpha z)$ ($\alpha$ arbitrary) disturbance, we can expect that such a disturbance interacts with the periodic corrugation via the base flow. This interaction causes the disturbance to be modulated as $\exp(\mathrm{i}(\alpha \pm k)z)$. The modulated disturbance continues interacting with the periodic base flow and generates further modulated waves as $\exp(\mathrm{i}(\alpha \pm nk)z)$ ($n = 1, 2, \cdots$). Since each individual wave pattern is clearly not a solution of the interfacial evolution equation, it is reasonable that the overall behaviour of numerous modulated disturbances can act as an envelope of a primary $2\pi/\alpha$–wavelength wave superimposed upon a secondary $2\pi/k$ (and all of its higher harmonics)–wavelength wave. Bloch functions are therefore the appropriate trial functions to describe the above phenomena and we employ them instead of Fourier modes.

Below, we invoke two procedures using Bloch-type functions. First, we solve an eigenvalue problem deriving from (4.5) and construct a solution to (4.5) using this theorem. Alternatively, we directly solve (4.5) numerically for various fixed initial wavelengths of the interfacial perturbations and see how the interface evolves in the presence of a corrugation. We then compare.

#### 4.4.1. *Eigenvalue problem*

Define the trial Bloch function

$$\xi(z,\tau) = \exp(\mathrm{i}\alpha z) \sum_{n=-\infty}^{\infty} \hat{\xi}_n \exp(\mathrm{i}nkz + \omega\tau), \tag{4.9}$$

as an eigenfunction of (4.5). $\omega$ is the eigenvalue or the complex growth rate arising in the temporal analysis (i.e. $\omega$ is the Laplace transform variable) and, for a monochromatic initial disturbance, $\alpha$ is the primary disturbance's wavenumber. The prefactor represents the disturbed flow and multiplies the base flow represented by $\exp(\mathrm{i}kz)$. Use of (4.9) guarantees a bounded solution in the $z$ (the axial coordinate) domain if (4.9) converges as $|n| \to \infty$ for each fixed instant $\tau$, and translates (4.5) into an infinite hierarchy of algebraic equations for the coefficients $\hat{\xi}_n$ and for $\omega$. If the wall function is a pure mode of wavenumber $k$, then from (3.8), $\eta - \phi = (\hat{\eta} - \hat{\phi})\,\mathrm{e}^{\mathrm{i}kz} + (\hat{\eta} - \hat{\phi})^*\mathrm{e}^{-\mathrm{i}kz}$

and this hierarchy becomes

$$\sigma Q^{-}(n)\hat{\xi}_{n-1} + (\omega + P(n))\hat{\xi}_n + \sigma Q^{+}(n)\hat{\xi}_{n+1} = 0, \tag{4.10}$$

where, by defining $\beta(n) = \alpha + nk$,

$$P(n) = \frac{2\mathrm{i}}{m}\beta(n) - \frac{J_0}{3m\lambda}\beta^2(n)(1-\beta^2(n)), \tag{4.11}$$

$$Q^{+}(n) = \mathrm{i}\beta(n)(\hat{\eta}-\hat{\phi})^{*}\left[\frac{4}{m} - \frac{J_0}{m\lambda}\mathrm{i}\beta(n+1)(1-\beta^2(n+1))\right], \tag{4.12a}$$

$$Q^{-}(n) = \mathrm{i}\beta(n)(\hat{\eta}-\hat{\phi})\left[\frac{4}{m} - \frac{J_0}{m\lambda}\mathrm{i}\beta(n-1)(1-\beta^2(n-1))\right]. \tag{4.12b}$$

Note that we can express (4.10) in terms of a tridiagonal matrix whose the principal and off-diagonal elements are $P(n)$ and $\sigma Q^{\pm}(n)$, respectively. Note also that $\sigma \ll 1$ means that this matrix is in fact a diagonal matrix perturbed along its principal super and subdiagonals only. If the wall function is an arbitrary function with period $2\pi/k$, the matrix may, in general, have all non-zero elements. The infinite hierarchy (4.10) has, in general, an infinite number of solutions $\omega$. We seek only the (dominant) eigenvalue with maximum real part.

(i) *Numerical solution of the eigenvalue problem.* The eigenvalue $\omega$ is determined by setting the determinant $D$ of (4.10) to zero, and will be a function of $J_0$, $\lambda$, $m$, $k$, $\sigma$ and $\alpha$. For a truncation at some value of $n$, we can calculate the eigenvalues of this matrix equation (4.10) numerically. We then increase $n$ until the dominant eigenvalues (not only the dominant one) no longer change significantly with $n$. In addition, as a check, we also apply determinant/matrix perturbation theory in $\sigma$ to determine the correction to the growth rate as the result of $\sigma \neq 0$. Since (4.9) implies that all wave patterns ($\alpha \pm nk$) should belong to the same growth rate, replacing $\alpha$ by $\alpha \pm k$ leaves $D$ in (4.10) unchanged. Thus the eigenvalue spectra are $k$-periodic in $\alpha$-space. One can also see this by noting that the coefficients in (4.5) are $k$-periodic. We thus need only calculate one (the 'primary') branch of the spectrum with respect to that at $\sigma = 0$, and we can then extend it periodically in $\alpha$.

(ii) *Martrix perturbation theory.* By expanding the determinant implied by (4.10) in $\sigma$, we have

$$D_0 + \sigma^2 D_2 + O(\sigma^4) = 0, \tag{4.13}$$

where

$$D_0 = \prod_j (\omega + P(j)), \quad D_2 = -\sum_n \prod_{j\neq n,n+1} (\omega + P(j))Q^{+}(n)Q^{-}(n+1).$$

Hence, we expect that the growth rate $\omega$ has an expansion in powers of $\sigma$:

$$\omega = \omega_0 + \sigma^2\omega_2 + O(\sigma^4). \tag{4.14}$$

The correction to the growth rate appears with coefficient $\sigma^2$ and should require observation times roughly of order $1/\sigma^2$ to be distinguished from the straight tube case. We require $\sigma \gg \varepsilon^{1/2}$ so that the $O(\varepsilon^2)$ terms from the straight tube PCAF analysis leading to (4.5) are of higher order than the leading-order corrugation correction.

To find $\omega_2$, we can use the solvability condition for the perturbed matrix equation, the Lindset–Poincare technique or matrix perturbation theory. For the latter, expand (4.13) about $\omega = \omega_0$ and note $D_0(\omega = \omega_0) = 0$ to find $\omega_2 = -D_2/(\partial D_0/\partial\omega)$ at $\omega = \omega_0$.

Noting that the $j = 0$ factors in $D_0$ and $D_2$ are $\omega_0 + P(0) = 0$, we can substitute for $D_0$ and $(\partial D_0/\partial\omega)$ at $\omega = \omega_0$ to obtain

$$\omega_2 = \frac{Q^+(0)Q^-(1)}{P(1)-P(0)} + \frac{Q^+(-1)Q^-(0)}{P(-1)-P(0)} = \|\hat{\eta} - \hat{\phi}\|^2 F(0)\left(\frac{F(1)}{P(1)-P(0)} + \frac{F(-1)}{P(-1)-P(0)}\right), \tag{4.15}$$

where

$$F(n) = \frac{4\mathrm{i}\beta(n)}{m} + \frac{J_0}{m\lambda}\beta^2(n)(1-\beta^2(n))$$

is a dispersion expression associated with $\alpha \pm nk$, i.e. by substituting (4.9) for $\xi$ into the $O(\sigma)$ part of (4.5) for an uncorrugated wall. Notice that $\omega_0 = -P(0)$ is the growth rate of the uncorrugated $\sigma = 0$ flow. The expressions $P(\pm1)$, $P(0)$, $F(\pm1)$ and $F(0)$ in (4.15) involve only the interactions between the primary disturbance's wavenumber $\alpha$ and its first harmonics $\alpha \pm k$. In fact, (4.15) follows simply by truncating (4.10) into a $3 \times 3$ matrix with respect to the central element $\omega + P(0)$, expanding the matrix and solving when $\sigma \ll 1$. The corrugated geometry is reflected by $\sigma\|\hat{\eta} - \hat{\phi}\|$. The numerators in (4.15) represent the off-diagonal interactions from the $O(\sigma)$ terms of (4.10). The term in the large parentheses, which we shall call $f$, in (4.15) can be understood as follows. Write the Laplace transform of (4.5) in operator notation as $\omega\xi + L\xi = 0$, let $\xi = \xi_0 + \sigma\xi_1 + \sigma^2\xi_2 + O(\sigma^3)$ and $L = L_0 + \sigma L_1 + O(\sigma^2)$. We can rederive (4.15) thus and show that the denominators originate from $L_0\xi_1$. They are related to the differences between eigenvalues, which encode information as to the time necessary for growth due to one branch to overtake growth due to the other.

(iii) *Growth rate correction in the long-wave limit*. Turning once again to the long primary wave regime (i.e. $\alpha \ll 1$), we can examine the correction to the growth rate in this limit. Its $\alpha$ expansion is

$$\omega_2 = \alpha\omega_2^{(1)} + \alpha^2\omega_2^{(2)} + O(\alpha^3). \tag{4.16}$$

As $\alpha \ll 1$, $\beta(n) \to \pm nk$. Thus, $F(\pm1)$ and $f$ depend only on the wall's wavenumber $k$ and $f$ is real-valued. When multiplied by the convective part $4\mathrm{i}\alpha/m$ of $F(0)$, it yields an $O(\alpha)$ growth correction

$$\omega_2^{(1)} = \frac{4\mathrm{i}}{m}\frac{\|\hat{\eta} - \hat{\phi}\|^2}{\Delta}\left(-\frac{2}{3}\left(\frac{J_0}{\lambda}\right)^2 C_k^2 + 16k^2\right). \tag{4.17}$$

Here, $C_k = k^2(1-k^2)$ is the contribution from the curvature of the base flow's interface and $\Delta = \frac{1}{9}(J_0/\lambda)^2 C_k^2 + 4k^2$. The $O(\alpha)$ growth correction is purely (imaginary) dispersive and a correction to the stability first occurs at $O(\alpha^2)$.

$$\omega_{2r}^{(2)} = \|\hat{\eta} - \hat{\phi}\|^2\left[\frac{J_0}{m\lambda\Delta}(-\tfrac{2}{3}(J_0/\lambda)^2 C_k^2 + 16k^2) + \frac{4}{m\Delta}\left(\frac{8J_0}{3\lambda}C_k + \frac{40J_0}{3\lambda}k^2(1-2k^2) - \frac{40C_k^2 q}{27\Delta}\right)\right]. \tag{4.18}$$

Here, $q = 2k^2(1-2k^2)$ is the $\alpha \to 0$ limit of the interaction of capillary terms from $\alpha$ and $\alpha \pm k$.

### 4.4.2. *Initial-value problem*

In order to confirm the stability behaviour predicted by the eigenvalue spectrum discussed above and to see the (linear) dynamics of the interface's evolution, including

the modulation of the initial wavelength with time, it is useful to solve the initial-value problem directly. To discretize the axial coordinate $z$, we employ a Bloch-type form in the sense of a spectral method, i.e.

$$\xi(z,\tau) = \sum_{n=-N}^{N} a_n(\tau)\cos((\alpha+nk)z) + b_n(\tau)\sin((\alpha+nk)z), \tag{4.19}$$

where $N$ is the mode number cutoff, subject to the initial condition $\xi(z,\tau=0) = \cos(\alpha z)$. $a_n(\tau)$ and $b_n(\tau)$ are amplitude functions that depend on $\tau$. Unlike the eigenvalue problem, $\xi$ is a linear combination of all eigenmodes rather than the single mode (4.9),

$$\xi(z,\tau) = \sum_j c_j\xi_j(z,\tau) \quad \text{where} \quad \xi_j(z,\tau) = \exp(\mathrm{i}\alpha z)\sum_{-\infty}^{\infty}\hat{\xi}_{jn}\exp(\mathrm{i}nkz+\omega_j\tau) \tag{4.20}$$

for the $j$th mode. Therefore, in terms of the initial-value problem, $a_n(\tau)$ and $b_n(\tau)$ should contain contributions from all possible eigenmodes and their asymptotic behaviour as $\tau\to\infty$ should correspond to the mode of the eigenvalue spectrum with the dominant growth rate. We retain only a finite number of modes. Substituting (4.19) into (4.5) leads to a system of ordinary differential equations for the amplitudes $a_n(\tau)$ and $b_n(\tau)$. We use a 12th-order Adam–Moulton algorithm from the IMSL library to solve these ODEs. For a fixed number $2N+1$ of modes, we determine the solutions $a_n(\tau)$ and $b_n(\tau)$ within a 0.1% absolute error tolerance and increase $N$ until the spatial evolution at a fixed time no longer changes significantly.

## 5. Results and discussion

### 5.1. *Eigenvalue spectrum*

Since (4.5) is linear, an arbitrary disturbance can be decomposed into a linear combination of functions that form a basis for $L^2(\mathbb{R})$, and the solution is the same linear combination of the responses to the functions in this set. We assume that the set of Bloch eigenfunctions of (the non-self-adjoint problem) (4.5) with periodic boundary conditions in $z$ forms such a basis and test a necessary condition for this by comparing the eigenvalue-based solution with the direct numerical solution of (4.5), both subject to the same initial conditions. A difference could signal a lack of completeness of the Bloch eigenfunctions. Using the methods outlined above for equation (4.5), we find features of the eigenvalue spectrum that are rather different from those of the straight tube. As we see in figure 4, the character of the eigenvalue spectrum shows the existence of a banded structure in which each band represents a continuous spectrum of the corresponding eigenvalue as a function of the initial disturbance's wavenumber $\alpha$. Such structures illustrate the $k$-periodicity in $\alpha$-space noted earlier.

The eigenvalue spectra (the real parts of eigenvalues here) are shown in figure 4 for different wall wavenumbers with dotted (the primary branch) and dashed (the secondary branch) curves. Note that since we introduce a long time scale $\tau=\varepsilon t$, the true eigenvalues should be $\varepsilon\omega$. For comparison, the solid lines in figures 4 represent the uncorrugated case for $\sigma=0$. In contrast to the uncorrugated case $\sigma=0$, most short-wave disturbances give rise to growth. For $k>2$, there are narrow gaps of stable wavenumber between the unstable branches in the short-wave spectrum. This eigenvalue spectrum represents the direct effects of capillarity and its interaction with

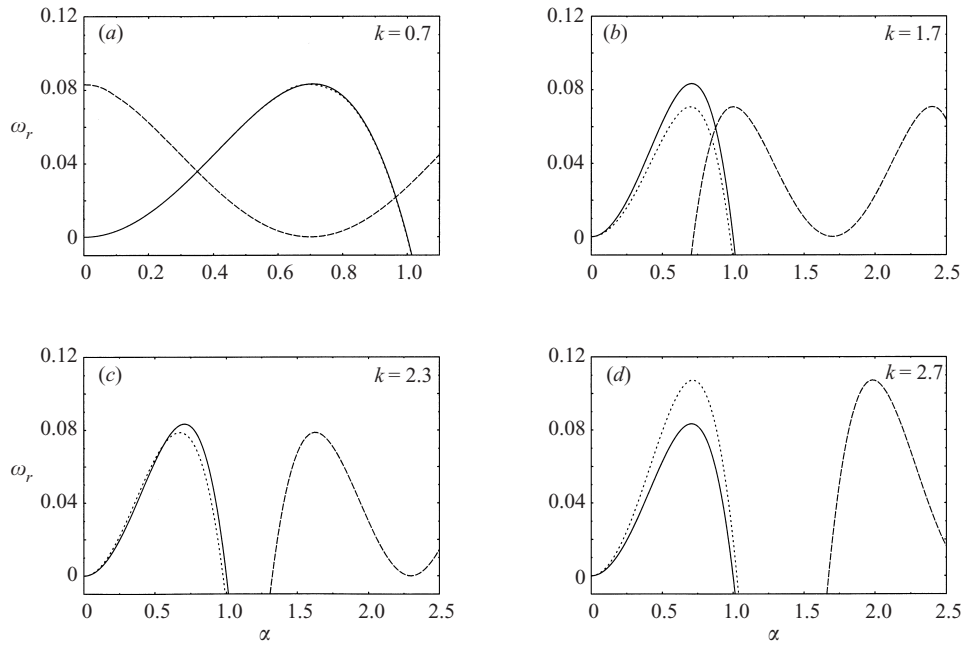


FIGURE 4. The eigenvalue spectrum (growth rate curves) for various $k$. $J_0/\lambda = 1.0$, $m = 1$, $\sigma = 0.2$, ——, $\sigma = 0.0$; $\cdots$, primary branch; – – –, 2nd branch.

the wall's harmonics $(\alpha + nk)$ (i.e. $\omega_r \sim (J_0/3m\lambda)(\alpha + nk)^2(1 - (\alpha + nk)^2) + O(\sigma^2)$). The maximum growth rate for a given initial disturbance wavenumber $\alpha$ depends on the relative position of the unstable branches. As we shall see, if the branch with the highest growth rate for $\alpha$ is not the primary branch, the long-time linear evolution may lead to the dominance of a wavelength other than $\alpha$. The initial-value calculation in the next section will confirm this behaviour. In addition to this effect of the periodic spectrum owing to corrugation, there is also an $O(\sigma^2)$ deviation of the primary branch from the straight tube growth rate. This latter correction can displace the critical wavenumber of the primary branch in either direction from its straight tube value of one.

### 5.2. *Interfacial evolution and growth rate correction*

Figures 5($a$) and 5($b$) show the interfacial evolutions at a particular position ($z = 0$) for different sets of initial and wall wavenumbers $(\alpha, k)$ with fixed $J_0/\lambda = 1$, $m = 1$ and $|\alpha - k| = 0.5$, corresponding to spectra in figures 4($a$) and 4($b$). Figure 5($a$) is the case of an initial long wavelength ($\alpha < 1$) disturbance and evolutions for both shorter and longer times are shown. The interface grows slowly until $\tau \approx 120$ when it begins a noticeable exponential growth. Notice that the frequency of the later development also becomes quicker. Figure 5($b$) shows the case of imposing a short wavelength initial disturbance that would be stable in an uncorrugated tube and has a negative growth contribution from the primary branch. Consequently, the short-wave disturbance decays initially; it then interacts with the corrugation (when $\tau \approx 10 \sim 20$) and leads to growth. The change from decaying to growth implies that the apparent dominant eigenmode has changed from short to long times owing to corrugation. The long-term linear interfacial behaviour corresponds to the mode with the dominant growth rate predicted by the eigenvalue spectrum. Thus, to identify which modes

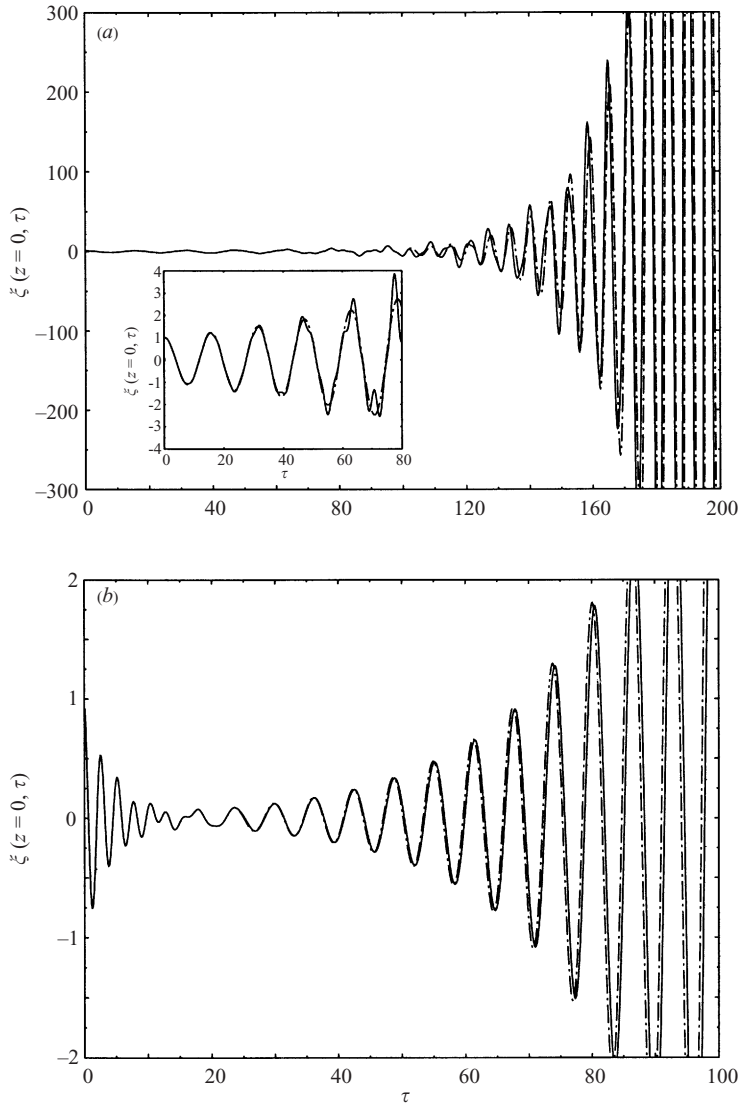


FIGURE 5. (*a*) The temporal behaviour of the interfacial amplitude at $z = 0$ for $\alpha = 0.2$, $k = 0.7$, $\sigma = 0.2$. (*b*) Temporal behaviour of the interface amplitude at $z = 0$, $\alpha = 1.2$, $k = 1.7$, $\sigma = 0.2$. ——, initial-value approach; – · –, eigenvalue approach.

contribute to the long-time evolution, we compare the solution of the initial-value problem with the functional form,

$$A\cos(\mathrm{Im}(\omega_{dominant})\tau + B)\exp(\mathrm{Re}(\omega_{dominant})\tau), \tag{5.1}$$

where $\omega_{dominant}$ is the eigenvalue with the largest real part discernable from the eigenvalue spectrum for the given $\alpha$ in figure 4. We choose the prefactor $A$ and phase angle $B$ by matching the profile from the moment at which it develops a clearly oscillatory/exponential pattern. Afterwards, as figure 5 indicates, the linear growth oscillates as $\mathrm{Im}(\omega_{dominant})$ and grows as $\mathrm{Re}(\omega_{dominant})$, as expected. The excellent agreement shows that $\omega_{dominant}$ belongs to the secondary eigenbranch.

Figures 6(*a*) and 6(*b*) are the spatial evolutions corresponding to figures 5(*a*) and

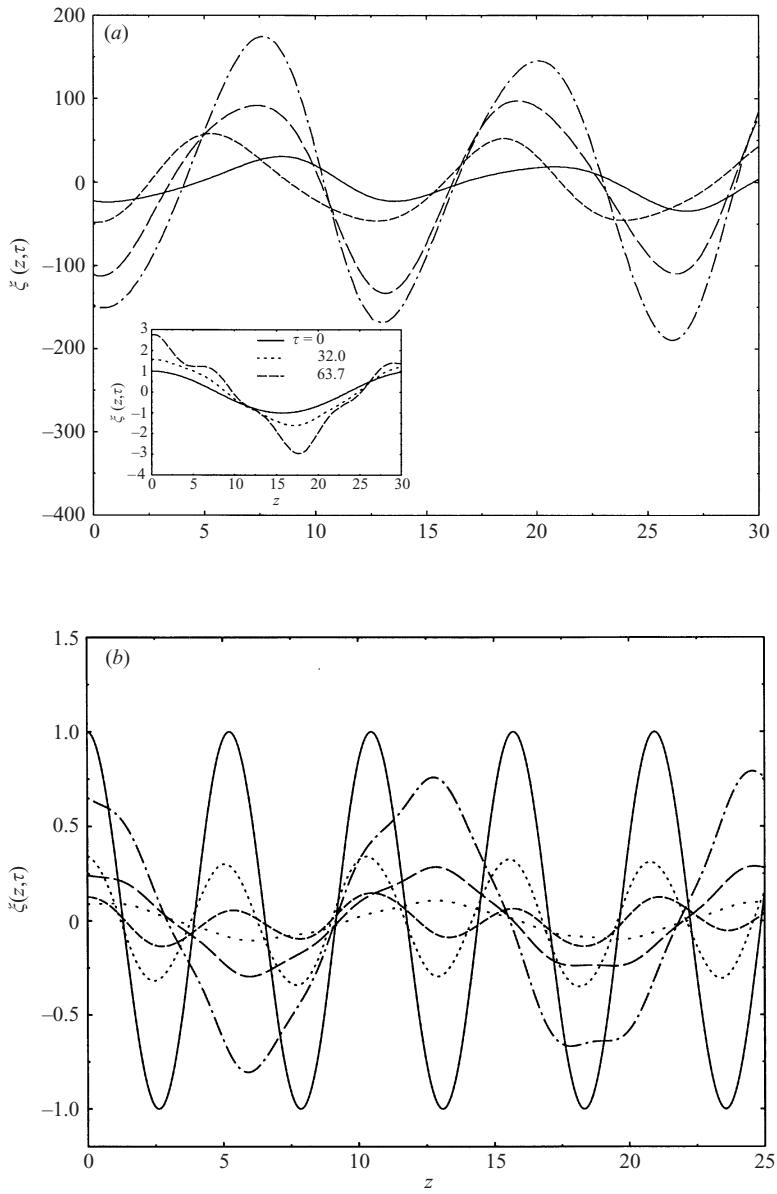


FIGURE 6. (*a*) The spatial evolutions for shorter (inset) and longer times for figure 5(*a*). $\alpha = 0.2$, $k = 0.7$, $\sigma = 0.2$, ——, $\tau = 131.1$; – – –, 142.7; — — ·, 155.8; · — ·, 162.2. (*b*) The corresponding spatial evolutions for various times for figure 5(*b*). $\alpha = 1.2$, $k = 1.7$, $\sigma = 0.2$. ——, $\tau = 0$; · · ·, 5.1; – – –, 10.4; • • •, 26.8; — — ·, 42.5; · — ·, 61.4.

5(*b*), respectively. There are a number of wavelengths that contribute to the observed evolution. Figure 6(*a*) begins with a long-wave initial disturbance. The wavelength ($\sim 12$) that dominates the later evolution is much shorter than the initial wave ($\sim 30$ for $\alpha = 0.2$). Its wavenumber of $0.5 = |\alpha - k|$ is just the first wall harmonic of the initial disturbance and characterizes the long-time (linear) behaviour. The long-time capillary growth rate numerically matches $(J_0/3m\lambda)(\alpha - k)^2(1 - (\alpha - k)^2)$ approximately, consistent with figure 5(*a*).

Similarly, in the case of a short-wave initial disturbance in figure 6(*b*), the short

wavelength disturbance decays at the earlier stage of the evolution, then gradually grows with a longer wavelength. The first harmonic interaction again leads to a predominant first harmonic's wavenumber of 0.5, but now this wavelength exceeds the initial value $\alpha = 1.2$. Therefore, in contrast to the straight tube, even an initial short wavelength disturbance can lead to the unstable growth of a long wave owing to the coupling to its higher wall harmonics through the corrugation. Figure 5(*b*) clearly indicates the transition between the decaying (primary) mode and growing first harmonic mode. By expressing the time-dependent solution in terms of all the eigenstates $f_j(z)$

$$\xi = a_p f_p(z)\exp(\omega_p \tau) + \sum_{branch\, j} a_j f_j(z)\exp(\omega_{\langle j\rangle}\tau), \tag{5.2}$$

we gain some insight. The subscript $p$ represents the primary branch, which is related to the uncorrugated $\sigma = 0$ stability. The coefficients $\{a_j\}$ are determined by the initial condition. Consider only the primary and secondary branches $j = 2$:

$$\omega_p = -\frac{2}{m}\mathrm{i}\alpha + \frac{J_0}{3m\lambda}\alpha^2(1-\alpha^2) + O(\sigma^2)$$

and

$$\omega_{\langle 2\rangle} = -\frac{2}{m}\mathrm{i}(\alpha - k) + \frac{J_0}{3m\lambda}(\alpha-k)^2(1-(\alpha-k)^2) + O(\sigma^2)$$

from our analysis. By defining the eigenvectors corresponding to the different eigenvalues, we can show that $a_p \sim O(1)$, $a_2 = a_{20}\sigma \sim O(\sigma)$. Therefore, the short-time evolution is governed by the primary branch. However, the secondary unstable branch can dominate for long times if $\mathrm{real}(\omega_p) < \mathrm{real}(\omega_{\langle 2\rangle})$ (note: $\mathrm{real}(\omega_p) < 0$ here) and the system stays in the linear regime. The transition implies there exists a critical time $\tau^* \approx \ln(q\sigma^{-1})/\mathrm{real}(\omega_{\langle 2\rangle} - \omega_p)$, when the amplitude of such a growing mode is about equal to that of the primary, i.e. $\sigma\exp(\omega_{(2)r}\tau^*) \sim q\exp(\omega_{Pr}\tau^*)$, when the growing mode becomes important and $q = (a_p/a_{20})(\|f_p\|/\|f_2\|)$. Thus, the smaller the corrugation or $\mathrm{real}(\omega_{\langle 2\rangle} - \omega_p)$, the later the transition, and short-wave disturbances remain stable longer. The parameter in figure 5(*b*) gives $\tau^* \approx 14$ for $q/\sigma \approx 10$, which predicts this onset of instability. Note that the time scale $\ln(1/\sigma)$ is shorter than $O(\sigma^{-1})$ estimated from the evolution equation (4.5).

For $\tau \ll \tau^*$, the primary branch dominates, and we may be interested in how its growth rate deviates from the $\sigma = 0$ case owing to corrugation. Figures 7(*a*) and 7(*b*) show the growth rate deviation $\delta\omega_r := \omega_{\mathrm{from(4.10)}} - \omega_{\sigma=0}$ for the primary branch, comparing the numerical and the analytical matrix perturbation results (Equation (4.16) gives its long-wave limit (dashed curves)). The comparison is very good and verifies that $\delta\omega_r$ is $O(\sigma^2)$ for small enough $\sigma$. However, as figure 7(*b*) shows, larger wall wavenumbers $k$ show larger discrepancies between the numerical and the matrix perturbation results at large $\sigma$. Since the off-diagonal elements in (4.10) may grow relative to the principal diagonal ones with increasing $k$, retaining the determinant perturbation equation (4.13) to $O(\sigma^2)$ is probably no longer adequate. To understand these curves, they should be viewed in conjunction with figure 4. For $k = 1.7$, the corrugation is slightly stabilizing for long waves ($\alpha \to 0$) and the primary branch crosses the $\sigma = 0$ curve for $\alpha > 1$ (not shown). Since $\delta\omega_r$ therefore crosses zero, i.e. has a neutral point at about $\alpha \approx 1.4$ for the chosen parameters independent of $\sigma$, the three curves in figure 7(*a*) all cross at some value of $\alpha \approx 1.4$. This is not the case in figure 7(*b*) since, as figure 4(*d*) shows, for $k = 2.7$, the corrugation is always

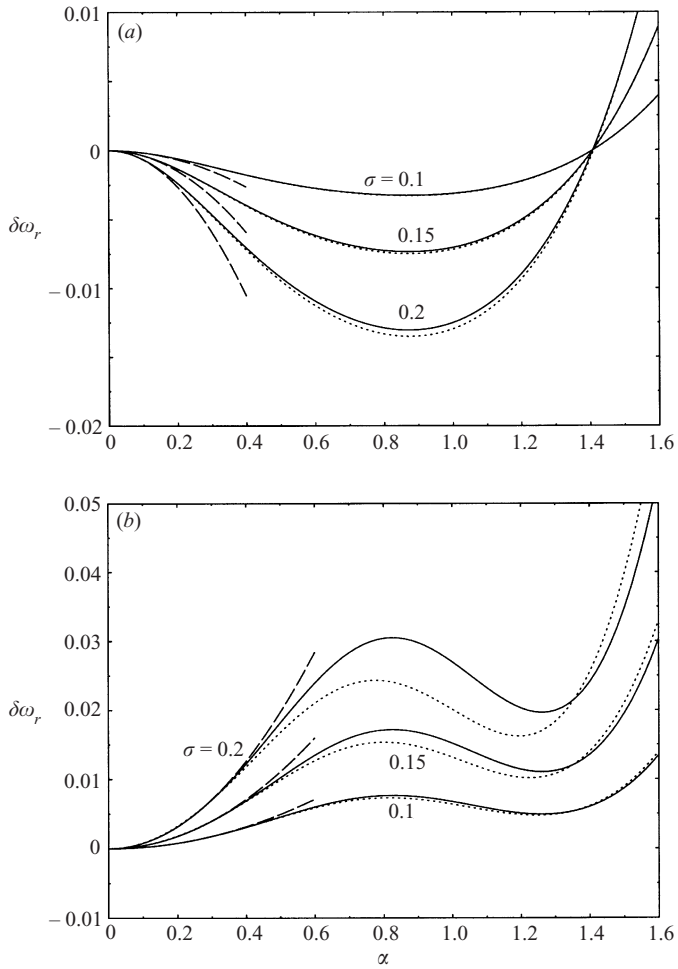


FIGURE 7. The growth rate correction due to various $\sigma$ for (*a*) $k = 1.7$ and (*b*) $k = 2.7$. $J_0/\lambda = 1.0$, $m = 1.0$. ——, numerical; · · ·, matrix perturbation; – – ·, long wave expansion of matrix perturbation.

destabilizing. From (4.15), all curves diverge as $\alpha^4$ for large $\alpha$, $\alpha \ll 1/\varepsilon$, as seen in figure 8. Thus, short $\alpha$-waves that would be stable in straight tubes are destabilized at order $\sigma^2$.

In conjunction with figure 4, let us examine how the growth rate correction $\sigma^2\omega_{2r}$ due to the corrugation varies with $k$ (figure 8) and $J_0/\lambda$ (not shown). From figure 8, the effect of corrugation disappears (for $\alpha$ not too large) for small $k$ since a long-wave wall corrugation appears essentially flat relative to a short $\alpha$-wave disturbance. Secondly, the curves for $k \gtrsim 2$ no longer have monotonic first derivatives. The real part of the $\alpha \to 0$ correction can change sign both with $k$ and with $J_0/\lambda$. For $k = 2.3$, $m = 2$, the $J_0/\lambda = 1, 2$ curves are similar to the $k = 2.3$ curve in figure 8, but the $J_0/\lambda = 3, 4$ curves begin with negative slopes. Equation (4.18) shows that the sign of $\omega_{2r}^{(2)}$ is a balance between the $k^2$-term originating from the shear flow and the factors involving the capillarity contribution $C_k J_0/\lambda$ from the wall's corrugation. It is zero at about $k \approx 2$ and for $J_0/\lambda = 1$. Since $\omega_{2r}(\alpha)$ apparently has a minimum everywhere in this parameter range, the sign of its $\alpha \to 0$ limit determines whether it has a maximum as well before approaching its $\alpha^4$ limit. Note that the entire corrugation is multiplied

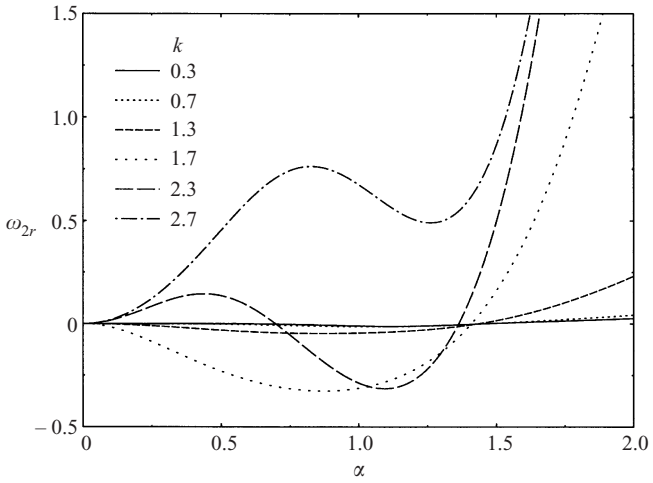


FIGURE 8. The effect of the wall wavenumber $k$ on the growth rate correction. $J_0/\lambda = 1.0$, $m = 1.0$.

by $\|\hat{\eta} - \hat{\phi}\|^2$, which is zero if the base state maintains a parallel flow as in the $k = 1$ case, and that both the capillary instability as well as it corrugation correction grow with $J_0/\lambda = 1/Ca_0$.

As noted, KT1 and KT2 have examined the stability of a core–annular flow in a corrugated tube, albeit in a very different parameter regime. Nevertheless, some trends that Kouris & Tsamopoulos observed are also apparent in (4.5). Figures 7 and 13 of KT2 are neutral curves (in our notation) in $m$ vs. the product of the wavenumber $k$, the Reynolds number $Re$ and $R_{2max}$, multiplied by an $O(1)$ correction due to their different choice of reference velocity. They show an increase in the stability region with decreasing $\varepsilon$, for parameters where $J/(mRe) \sim 5Re$. Thus, if $Re \sim \varepsilon$, then $J/(mRe) \sim \varepsilon$, unlike our situation of $J/(mRe) \sim \varepsilon^{-2}$. In this regime, decreasing $\varepsilon$ decreases $J/(mRe)$, which decreases the strength of the destabilizing capillarity in (4.5). Their figures 10 and 17, the effects of lowering the inverse Weber number or $J$, has a similar effect on $J/(mRe)$ and on the system's stability. Kouris & Tsamopoulos carry out their numerical calculations on a domain that is presumed periodic in the axial direction $z$ and find that increasing the length of the periodic domain in the calculation from one to five wall wavelengths results in a smaller stability region. This result is consistent with the Ansatz of the Floquet–Bloch analysis. In particular, this analysis provides that an initial disturbance $\alpha$, say one that would be stable in the absence of capillarity, can interact with the wall's periodicity $k$, as it flows through its crests and troughs, and excite waves $\alpha \pm nk$. This can only develop if the disturbance is allowed to progress through ($n$) wall waves before being renormalized by the enforced periodicity. Finally, the calculated eigenfunctions in KT2 (see e.g. KT2, figure 8) are long-wave dominant, with superimposed higher modes, not unlike the Bloch eigenfunctions of (4.9). The Bloch eigenfunctions that dominate at long times and thus dictate the long-time interfacial shapes in figures 6($b$) and 12 show qualitatively similar features, but with weaker higher modes, probably due to the corrugation's weakness in our calculation.

The analysis thus far has presumed $J/Re_1 \sim 1/\varepsilon^2$. However, either a stronger or a weaker scaling for $J/Re_1$ can significantly change the stability characteristics. Fortunately, we can extend the previous analysis to both stronger and weaker capillary cases with only minor changes.

### 5.3. *Very strong interfacial tension case, $\varepsilon^2 J/Re_1 \gg 1$*

As discussed in the base flow, a very strong interfacial tension, i.e. $\varepsilon^2 J/Re_1 \gg 1$ (here $J_0/\lambda \gg 1$) can smooth the base flow's interface. Let $S = J_0/\lambda = \varepsilon^2 J/Re_1$. Recall from equation (3.6), a strong interfacial tension $S \gg O(1)$ generates a flat interface to leading order with a correction of order $S^{-1}$, i.e. a deviated base state film thickness of $\eta - \phi = -\phi + O(S^{-1})$, owing to the flatter interface. Its stability follows from (4.5). The convective term (from the film's base flow) $(2/m)\xi_z$ becomes small relative to capillarity $\frac{1}{3}S(\xi_{zz} + \xi)_{zz}$ at $O(\sigma^0)$, and $(4/m)\xi \ll (S/m)(\xi_{zzz} + \xi_z)$ at $O(\sigma)$. For $\sigma S \gg O(S^0)$, the base flow is absent from the leading order. With the flatter interface, a rescaling of time brings the time derivative to $O(S)$,

$$S\left[\xi_{\tau'} + \frac{1}{3m}(\xi_{zz} + \xi)_{zz} + \frac{\sigma}{m}(\phi(\xi_{zz} + \xi)_z)_z\right] + O(S^0) = 0. \tag{5.3}$$

Therefore, the interfacial evolution reduces to that of the static, no-flow case to the leading order in $\varepsilon$, which is the linearized form of Hammond's equation (1983) corrected for a corrugated tube. Capillarity dominates over flow and $P(n)$ reduces to $-C(n) = -(S/3m)\beta^2(n)(1 - \beta^2(n))$ (see 4.11). $\hat{\eta}$ drops out to yield the growth rate correction (4.15) and its $\alpha \to 0$ expansion in this large $S$ limit:

$$\omega_2 = \frac{3S}{m}\|\hat{\phi}\|^2 C(0)\left(\frac{C(1)}{C(0) - C(1)} + \frac{C(-1)}{C(0) - C(-1)}\right) + O(S^0), \tag{5.4}$$

$$\omega_2 = -6\|\hat{\phi}\|^2 \frac{S}{m}\alpha^2 + O(\alpha^3) \quad \text{for} \quad \alpha \to 0. \tag{5.5}$$

Large $k$ or high tension enhances the effects of $C(\pm 1)$. Here, corrugations ($\|\hat{\phi}\| \neq 0$) make an $O(\sigma^2)$ stabilizing contribution to the $O(1)$ unstable long waves that is independent of $k$, except for the implicit dependence through $\|\hat{\phi}\|^2$. The reason is that for $k \gg \alpha$, corrugation simply adds a short wavelength component to the disturbance, which capillarity stabilizes.

In the absence of the base flow at leading order, an interesting phenomenon occurs. Since $\phi$ still appears in (5.3), the spectrum will still be $k$-periodic and there will be points where different branches cross, and thus where (5.4) breaks down. Obviously, (5.4) is not applicable there since its denominator becomes comparable to $\sigma^2$. This leads to an $O(\sigma)$ resonant correction to the growth rate. Particularly when $k < 2$ and such resonances occur at $\alpha$ in the long-wave regime whose the growth rate is positive, the corrugation can destabilize more significantly than the usual case where the base flow enters at leading order. To illustrate, we restrict our attention to $1 < k < 2$ and consider a resonance that occurs at $\alpha = \frac{1}{2}k$ in the long-wave regime. Since there may be corrections of different orders for a given range of $\alpha$, we use an iterated perturbation scheme (see the Appendix for details) to solve the following modified determinant equation and to obtain the maximum growth rate in this range of $\alpha$:

$$\left(\omega - \frac{S}{3m}C(0)\right)\left(\omega - \frac{S}{3m}C(1)\right)\left(\omega - \frac{S}{3m}C(-1)\right) + \sigma^2 G_2(\omega_0) = 0, \tag{5.6}$$

where

$$G_2(\omega_0) = -\left(\frac{S}{m}\right)^2 \|\hat{\phi}\|^2 C(0)\left(C(1)\left(\omega_0 - \frac{S}{3m}C(1)\right) + C(-1)\left(\omega_0 - \frac{S}{3m}C(1)\right)\right),$$

and $\omega_0$ is the $O(\sigma^0)$ eigenvalue of either the primary ($= -C(0)$) or the secondary

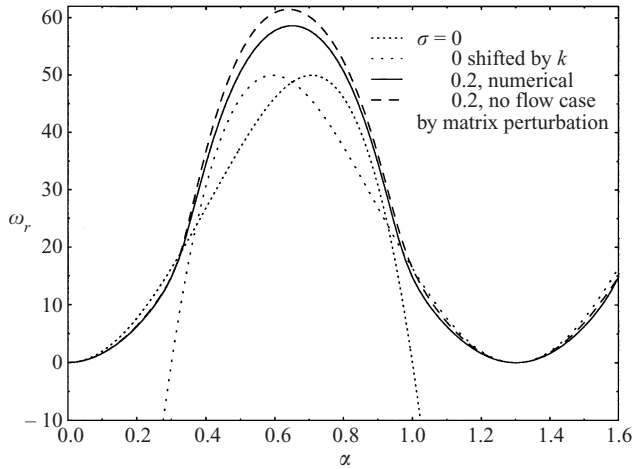


FIGURE 9. The growth rate as $J_0/\lambda = 600$, $m = 1$, $k = 1.3$, $\sigma = 0.2$.

branch ($= -C(-1)$). For $\alpha \approx \frac{1}{2}k$, $C(0) \approx C(-1)$, this gives,

$$\left(\omega - \frac{S}{3m}C(0)\right)^2 \approx -\sigma^2 G_2(\omega_0)\left(\omega_0 - \frac{S}{3m}C(1)\right)^{-1},$$

for the $O(\sigma)$ correction to the primary branch. This correction is one order larger in $\sigma$ than the correction that occurs when the base flow enters at leading order. A typical growth rate correction for this very high-tension case is shown in figure 9. The comparison between the direct numerical results of the matrix equation (4.10) and those of the asymptotic equation (5.6) is very good and confirms the enhanced unstable correction excited by this resonance.

### 5.4. *Moderately strong interfacial tension case, $\varepsilon \ll \varepsilon^2 J/Re_1 \ll 1$*

In the straight-tube case, it is well known (Chen & Joseph 1991; Georgiou *et al.* 1992) that a strong base flow can prevent the capillary instability where the core flow enters the leading order interfacial stability problem. Let us examine what happens when we decrease the strength of capillarity relative to shear for the corrugated case. Let $\varepsilon \ll \varepsilon^2 J/Re_1 \ll 1$, which magnifies the relative importance of the shear flow. Recall (equation (3.6)) that the base interface follows the wall (i.e. $\eta = \phi$) and the film becomes of uniform thickness with a resulting local parallel flow to the leading order in $\sigma$ and $S$. For $\varepsilon \ll S \ll 1$, corrugation impacts the leading-order stability only indirectly via the deflection of the base flow's film thickness $\sigma(\eta - \phi) \approx -\frac{1}{6}\sigma S(\phi_{zzz} + \phi_z) = O(\sigma S)$. An explicit corrugation correction must then be $O(\sigma\varepsilon S)$. Without significant change from the previous analysis, we can expand (4.5) and its base flow in $S$ to obtain:

$$\xi_\tau + \frac{2}{m}\xi_z + S\left[\frac{1}{3m}(\xi_{zz} + \xi)_{zz}\right] - \sigma S\left[\frac{2}{3m}(\phi_{zzz} + \phi_z)\xi\right]_z + O(\varepsilon S, \sigma S^2) = 0. \tag{5.7}$$

Since there is no translational symmetry due to the wall's corrugation, shear contributes to leading order. Capillarity comes in at $O(S)$ and corrugation at $O(\sigma S)$. The growth rate correction (4.15) is

$$\omega_2 = S^2 k^2 (1 - k^2)\|\hat{\phi}\|^2 \frac{4\mathrm{i}\alpha}{9m} + O(S^3) \tag{5.8}$$

in powers of $S$. Corrugation enters $\omega$ at $O(\sigma^2 S^2)$ in a purely dispersive manner and becomes non-dispersive only at the very high order $O(\sigma^2 S^3)$; it has very little impact. Higher-order contributions such as $O(\varepsilon S)$ from the straight-tube PCAF will be comparable to such corrugation corrections unless $\sigma^2 S^2 \gg \varepsilon$, which would be restricted to extremely thin films.

As Georgiou *et al.* (1992) and Papageorgiou *et al.* (1990) have shown for straight tubes, a surface tension $S = \varepsilon^2 J/Re_1 \sim \varepsilon$ couples the core to the leading-order interfacial stability, which for $m < 1$ can lead to a shear/viscosity stratification that can stabilize long waves. With corrugation, a derivation similar to that leading to (4.5) gives the evolution equation, inclusive of core-coupling (see Wei 2000 for details),

$$\xi_\tau + \frac{2}{m}\xi_z + \frac{\varepsilon J_0}{3mRe_1}(\xi_{zz} + \xi)_{zz} + \frac{\varepsilon}{2m}\gamma_z - \sigma\varepsilon\left[\left(\frac{2}{3m}(\phi_{zzz} + \phi_z) - \frac{\bar{\gamma}}{2m}\right)\xi\right]_z + O(\varepsilon^2, \sigma^2\varepsilon) = 0, \quad (5.9)$$

where $J_0$ and $Re_1$ are $O(1)$, $\gamma$ and $\bar{\gamma}$ represent the shear coupling from the disturbed and base core flow, respectively. As in (5.7), the corrugation's growth rate correction is $O(\sigma^2\varepsilon^3)$, of even higher order than the $O(\varepsilon^2)$ contribution from PCAF theory here, and is probably negligible.

### 5.5. *A wall with multiple length scale corrugations*

Pore waviness usually includes many wavelengths and its shape can be decomposed in terms of Fourier components in such cases. It may lead to multiple modulations due to an eigenvalue spectrum with multiple periodicities. As an example, we consider a wall that has corrugations with two wavenumbers, say, $(k_1, k_2) = (1.6, 2.4)$ and (2.4, 3.2). We have chosen these pairs to have the greatest common denominator $k = 0.8$ so as to yield identical long-time dominant waves. The corrugated base flow is (equation (3.6)) the superposition of the two individual wall wave patterns for the same $J_0/\lambda$, $m$, $\sigma$. The linear stability reduces to a pentadiagonal matrix eigenvalue problem.

$$\sigma Q_2^-(n)\hat{\xi}_{n-1} + \sigma Q_1^-(n)\hat{\xi}_{n-2} + (\omega + P(n)) + Q_1^+(n)\hat{\xi}_{n+1} + \sigma Q_2^+(n)\hat{\xi}_{n+2} = 0, \quad (5.10)$$

where $Q_s^\pm(n) = Q^\pm(n)$ for $k \to sk$ for $s = 1, 2$. The traces of the largest eigenvalues as functions of $\alpha$ for both $(k_1, k_2) = (1.6, 2.4)$ and (2.4, 3.2) are shown in figure 10. Recall from the single wavelength wall, the growth rate of the secondary branch may be higher than that of the primary branch. For $k > 2$ the growth rates there have $\alpha$-bands that are stable and a judicious choice of excitation wavelength $\alpha > 1$ can lead to a stable response. Figure 10 reveals that, for the pairs of $k$ chosen, no such gaps persist, despite their appearance in each (2.4 or 3.2) monochromatic wall's spectrum. Moreover, as $(k_1, k_2) = (2.4, 3.2)$ shows, the peaks need not be symmetric.

In order to confirm the above eigenvalue spectra and understand two-wall wavelength interactions, we again adopt the initial-value approach. The initial interface profile is $\xi(z, \tau = 0) = 0.1\cos(\alpha z)$. The initial wavenumber $\alpha$ for both cases is 0.2, within the range in which the growth rate of the primary branch is quite small and the non-primary branch is expected to dominate. The interfacial evolutions at $z = 0$ for $(k_1, k_2) = (1.6, 2.4)$ is shown in figure 11. Comparison between the long-time evolution of the initial-value approach and the maximum growth predicted by the Bloch function method again shows excellent agreement. For $(k_1, k_2) = (1.6, 2.4)$, the interface grows slowly before a transition signalling the dominance of the secondary branch occurs at $\tau \approx 80$. The later development shows faster growth and oscillation

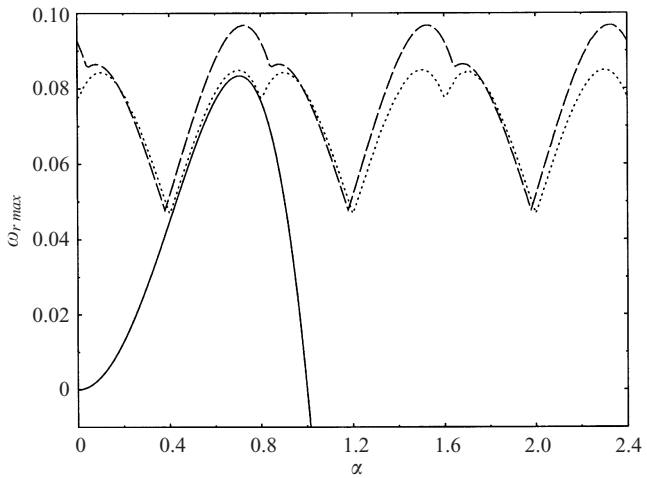


FIGURE 10. The growth rate in the presence of two wall wavelengths for $\sigma = 0.2$. ——, $(k_1, k_2) = (1.6, 2.4)$; – – –, $(k_1, k_2) = (2.4, 3.2)$.

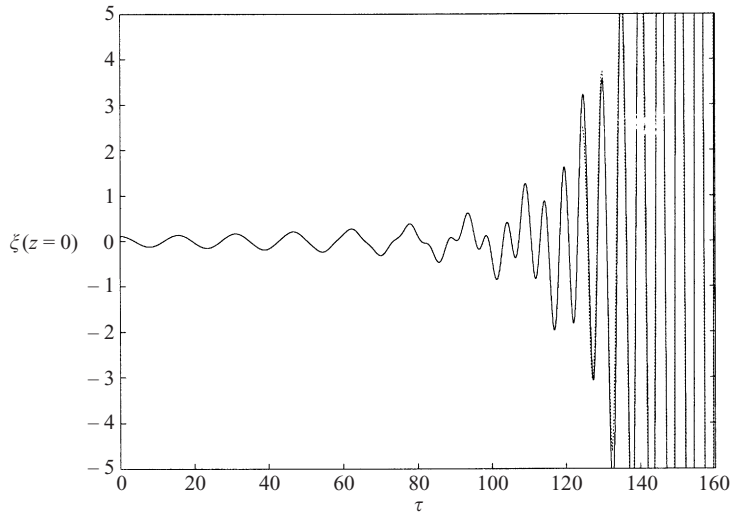


FIGURE 11. The interfacial evolutions at $z = 0$ for $(k_1, k_2) = (1.6, 2.4)$. $\alpha = 0.2$, $\sigma = 0.2$. ——, initial value approach; · · ·, Bloch growth rate.

than the earlier portion. The case of $(k_1, k_2) = (2.4, 3.2)$ (not shown) is very similar, but the transition occurs at $\tau \approx 50$. Thus, the fastest growing modes have been changed after interaction and, as we shall see below, the corresponding wave patterns change concurrently.

The entire interfacial evolutions in space are shown in figure 12 for $(k_1, k_2) = (1.6, 2.4)$. The interfacial evolution grows with the initial wavelength from the primary branch at the earlier stage of evolution, then interacts with the corrugations, where a shorter wavelength with a faster growth takes over for long times. For $(k_1, k_2) = (2.4, 3.2)$ (not shown) the evolution and the long-term growth are similar, but the transition takes place earlier. The wavenumber of the fastest growing mode in both cases is about 0.6 because the initial wave $\alpha$ has been modified to be $|\alpha + k_1 - k_2|$. This wave's growth rate dominates those of the other harmonic modes. It also explains the meaning of the non-primary branch for small $\alpha$ in figure 10.

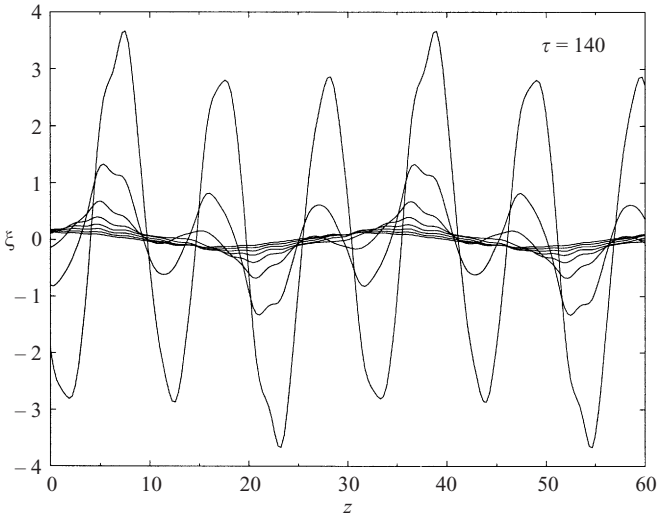


FIGURE 12. The corresponding spatial evolutions for the case in figure 11. $\alpha = 0.2$, $(k_1, k_2) = (1.6, 2.4)$, $\sigma = 0.2$.

### 5.6. *Application to oil recovery*

As a typical example of a liquid–liquid displacement, consider an oil film of $\mu_2 = 10\,\text{cP}$ surrounding a water slug ($\mu_1 = 1\,\text{cP}$) with an interfacial tension of $10\,\text{dyne cm}^{-1}$ in a 200 μm diameter pore. A typical velocity of a slug is about $1\,\text{cm s}^{-1}$. According to Bretherton (1961), the film thickness should go as a constant times $Ca^{2/3}$, or $\sim 3\,\mu\text{m}$. Consider a film thickness of 10 μm or $\varepsilon \sim 0.1$. These numbers give $J/Re_1 \sim 1000$ with $Re_1 \sim 1$ and $J \sim 1000$, which is within the range of our analysis. With these parameters, the straight cylindrical pore theory gives a maximum growth rate of $0.05\,\text{min}^{-1}$, i.e. about a 14 min doubling time, with wavelength 888 μm and a wave speed of $200\,\mu\text{m s}^{-1}$ for $\alpha_{max} = 0.707$ with a critical wavenumber of one. Consider a sinusoidal (one-wavelength) corrugation, of small amplitude, say 1.0 μm (still detectable), giving $\sigma = 0.1$, and a wall wavelength of 350 μm ($k_1 = 1.8$), shorter than the mean pore circumference of 628 μm. Consider now a short-wave disturbance of 500 μm or $\alpha = 1.26 > 1$, which would be stable in a straight tube. With the given corrugation, this perturbation excites an unstable wave of $\alpha' = |1.26 - 1.8| = 0.54$ or $L = 1164\,\mu\text{m}$ with a growth rate of $0.04\,\text{min}^{-1}$. This is the major effect of corrugation at these scales. In addition, there is a more minor effect from the perturbation of the primary branch which modifies the maximum growth rate to $0.048\,\text{min}^{-1}$ and hardly changes the wave speed. It also shifts the critical wavenumber for the primary branch to 0.99309 from 1. If the wall wavelength is equal to the pore diameter of 200 μm ($k = \pi$), then the maximum growth rate is slightly larger at $0.055\,\text{min}^{-1}$ and its wave speed is $204\,\mu\text{m s}^{-1}$.

## 6. Summary and conclusions

We use asymptotic methods to study the effect of small pore corrugation on the base flows and the corresponding linear stability of a core–annular flow for low capillary numbers and thin annulus films, i.e. $J/Re_1 = 1/Ca \sim 1/\varepsilon^2$. The small parameters are the scaled film thickness $\varepsilon$ and corrugation strength $\sigma$. We show that both the leading-order base flow and its leading-order stability are film-determined in

this limit, and the core's dynamics slaves those of the film. This is the advantage of treating the effect of corrugation in the two-fluid core–annular situation having a thin annular film, rather than with only a single fluid. It also allows, with rescaling to a different non-dimensionalization, application to a gas core. The film dynamics remain unchanged for slow or intermediate fluid motion, even though the core motion may be modified.

Corrugation does not only modify the magnitude (at $O(\sigma^2)$) of the unstable branch of eigenvalues that appears in the straight-tube case and thereby changes its critical wavenumber. Owing to the (wall wavenumber) $k$-periodicity of the spectrum in (disturbance wavenumber) $\alpha$-space, it also introduces other unstable branches to the eigenvalue spectrum. For example, in the straight-tube case, a short wavelength monochromatic disturbance simply decays with unchanged wavelength. In contrast, in the corrugated tube case for $k < 2$, the short-wave initial disturbances are stabilized at short times, but they excite unstable long waves via coupling to the corrugation harmonics for longer times of $O(\ln(1/\sigma))$. For $k > 2$, however, there are stable short-wave gaps between the adjacent branches and certain initial short waves will not excite unstable long waves, although others will. Since real systems contain more than one wall wavelength, this stable gap may no longer appear owing to an interaction between different wall wavelengths. Therefore, real pore systems are rarely linearly stable to any order-one wavelength disturbances.

The theory can be extended to the range of $J/Re_1 \gg 1/\varepsilon$. The stability of the very strong surface tension case, i.e. $J/Re_1 \gg 1/\varepsilon^2$, reduces to the no-flow limit because of the relatively weak strength of the base film flow. The corrugation can contribute a stability $O(\sigma)$ correction to the primary branch growth rate in some ranges of parameters owing to a resonance. For less strong tension as $1/\varepsilon \ll J/Re_1 \ll 1/\varepsilon^2$, the growth rate correction is $O(\sigma^2 S^3)$ where $S = \varepsilon^2 J/Re_1$; at this order, corrugation effects are negligible compared with non-leading order straight-tube corrections. At $J/Re_1 \sim 1/\varepsilon$, however, the dynamics of the core contribute to determining the interfacial shape in the base flow as well as to the system's linear stability, but the corrugation effect on the growth rate is rather negligible.

Kouris & Tsamopoulos (KT1, KT2) numerically solve for the steady-state flows and the linear stability of a core–annular flow in a sinusoidally varying tube for low tension ($J/(mRe) \sim \varepsilon$ or 1) and typically large $Re$ where viscosity stratification is the major source of instability. Whereas most of their calculations are beyond the reach of our theory, a number of their observed parameter trends, both in the steady interfacial shape and in the system's stability, are qualitatively apparent in our equations. Of course, the development of an asymptotic theory similar to the above, but where the core does not slave the film (as needed, e.g. for viscous stratification to play a leading-order effect (Papageorgiou *et al.* 1990)) would be desirable. Unfortunately, for $m = O(1)$, scalings that result in a leading-order core contribution do not have $O(\sigma)$, i.e. corrugation, corrections at leading order. Thus, the most promising way for the core-coupling to become significant is when the core fluid is much more viscous than the film fluid, say $m \sim O(\varepsilon)$ as in KT. Here, core-coupling should be expected for both the base flow and its stability. As noted, a very weakly viscous film fluid destroys lubrication in the film, and thereby significantly alters the analysis. This will be the subject of a future paper.

We would like to thank the Donors of the Petroleum Research Fund for supporting this work under grant PRF#27403-AC9,2.

## Appendix

For $S \gg 1$, the Bloch determinant is (4.10) with slightly changed definitions of (4.11)

$$P(n) = -\frac{S}{3m}\beta^2(n)(1-\beta^2(n)), \tag{A 1b}$$

$$Q^+(n) = -\hat{\phi}^*\frac{S}{m}\beta(n)\beta(n+1)(1-\beta^2(n+1)), \tag{A 1b}$$

$$Q^-(n) = -\hat{\phi}\frac{S}{m}\beta(n)\beta(n-1)(1-\beta^2(n-1)). \tag{A 1b}$$

For $0 \leqslant \alpha < k$ with $k > 1$, $\omega + P(0)$ (the primary $\alpha$-branch) and $\omega + P(-1)$ (the secondary $(\alpha - k)$ branch) at the $O(\sigma^0)$ determinant $D_0$ give the same $\omega_0$ at $\alpha = \frac{1}{2}k$. Also, $\omega + P(1)$ (the secondary $(\alpha + k)$ branch) and $\omega + P(-1)$ have the same $\omega_0$ at $\alpha = 0$. These multiplicities contribute at $O(\sigma)$ to the growth rate correction rather than at $O(\sigma^2)$.

To solve for $\omega$ by taking the interaction between these three branches into account regardless of the range of $\alpha$, we rearrange the determinant $D$. We first extract $\omega+P(0)$, $\omega + P(-1)$, and $\omega + P(1)$ from $D_0$ as the $O(\sigma^0)$ determinant, and combine the other terms of $D_0$ with $D_2$ into the $O(\sigma^2)$ contribution:

$$G_0(\omega) + \sigma^2 G_2(\omega) = 0, \tag{A 2}$$

$$G_0 = (\omega + P(-1))(\omega + P(0))(\omega + P(1)), \quad G_2 = D_2 \Big/ \prod_{j\neq 0,\pm 1} (\omega + P(j)). \tag{A 3a,b}$$

$G_0$ contains the primary and both secondary branches. We solve (A2) for $\omega$ by an iteration scheme by evaluating $G_2$ at $\omega = \omega_0$ or $G_0(\omega) + \sigma^2 G_2(\omega_0) = 0$. For figure 9, we choose $\omega_0$ as $-P(0)$ for $0 \leqslant \alpha \leqslant \frac{1}{2}k$, and as $-P(-1)$ for $\frac{1}{2}k \leqslant \alpha < \frac{3}{2}k$ to find the maximum growth rate.

## REFERENCES


Abramowitz, M. & Stegun, I. A. 1972 *Handbook of Mathematical Functions*. Dover.

Bretherton, F. P. 1961 The motion of long bubbles in tubes. *J. Fluid Mech.* **10**, 166–188.

Chandrasekhar, S. 1968 *Hydrodynamic and Hydromagnetic Stability*. Oxford University Press.

Chen, K., Bai, R. & Joseph, D. D. 1990 Lubricated pipelining. Part 3. Stability of core–annular flow in vertical tubes. *J. Fluid Mech.* **214**, 251–286.

Chen, K. & Joseph, D. D. 1991 Long waves and lubrication theories for core annular flow. *Phys. Fluids* A **3**, 2672–2679.

Chow, J. C. F. & Soda, J. 1972 Laminar flow in tubes with constriction. *Phys. Fluids* **15**, 1700–1706.

Coward, A. V., Papageorgiou, D. T. & Smyrlis, Y. S. 1995 Nonlinear stability of oscillatory core–annular flow: a generalized Kuramoto–Sivashinsky equation with time periodic coefficients. *Z. Angew. Math. Phys.* **46**, 1–39.

Dassori, C. G., Deiber, J. A. & Cassano, A. E. 1984 Slow two-phase flow through a sinusoidal channel. *Intl J. Multiphase Flow* **10**, 181–193.

Gauglitz, P. A. & Radke, C. J. 1988 An extended evolution equation for liquid film break up in cylindrical capillaries. *Chem. Engng Sci.* **43**, 1457–1465.

Gauglitz, P. A. & Radke, C. J. 1990 The dynamics of liquid film break up in constricted cylindrical capillaries. *J. Colloid Interface Sci.* **134**, 14–40.

Georgiou, E., Maldarelli, C., Papageorgiou, D. T. & Rumschitzki, D. S. 1992 An asymptotic theory for the linear stability of a core–annular flow in the thin annular limit. *J. Fluid Mech.* **243**, 653–677.

Halpern, D. & Grotberg, J. B. 1993 Surfactant effects on fluid-elastic instabilities of liquid-lined flexible tubes: a model of airway closure. *J. Biomech. Engng* **115**, 271–277.

Hammond, P. S. 1983 Nonlinear adjustment of a thin annular film of viscous fluid surrounding a thread of another within a circular cylindrical pipe. *J. Fluid Mech.* **137**, 363–384.

Hickox, C. E. 1971 Instability due to viscosity and density stratification in axisymmetric pipe flow. *Phys. Fluids* **14**, 251–262.

Hu, H. H. & Joseph, D. D. 1989 Lubricated pipelines: stability of core–annular flow. Part 2. *J. Fluid Mech.* **205**, 359–396.

Hu, H. H., Lundgren, T. & Joseph, D. D. 1990 Stability of core–annular flow with a small viscosity ratio. *Phys. Fluids* A **2**, 1945–1954.

Joseph, D. D., Renardy, Y. & Renardy, M. 1984 Instability of the flow of immiscible liquids with different viscosities in pipe. *J. Fluid Mech.* **141**, 309–317.

Kang, F. & Chen, K. 1995 Gravity-driven two-layer flow down a slightly wavy periodic inclined plane at low Reynolds number. *Intl J. Multiphase Flow* **21**, 501–513.

Kelly, E. 1967 On the stability of an inviscid shear layer which is periodic in space and time. *J. Fluid Mech.* **27**, 657–689.

Kouris, C. & Tsamopoulos, J. 2000 Concentric core–annular flow in a periodically constricted circular tube. Part 1. Steady-state, linear stability and energy analysis. *J. Fluid Mech.* **432**, 31–68.

Kouris, C. & Tsamopoulos, J. 2001 Concentric core–annular flow in a circular tube of slowly varying cross-section. *Chem. Engng Sci.* **55**, 5509–5530.

Otis, D. R., Johnson, M., Pedley, T. J. & Kamm, R. D. 1993 The role of pulmonary surfactant in airway closure. *J. Appl. Physiol.* **75**, 1323–1333.

Papageorgiou, D. T., Maldarelli, C. & Rumschitzki, D. S. 1990 Nonlinear interfacial stability of core–annular film flows. *Phys. Fluids* A **2**, 346–352.

Park, C. W. & Homsy, G. M. 1984 Two-phase displacement in Hele-Shaw cells: theory. *J. Fluid Mech.* **139**, 291–308.

Pozrikids, C. 1988 The flow of a liquid film along a periodic wall. *J. Fluid Mech.* **188**, 275–300.

Preziosi, K., Chen, K. & Joseph, D. D. 1989 Lubricated pipelines: stability of flow. *J. Fluid Mech.* **201**, 323–356.

Ransokoff, T. C., Gauglitz, P. A. & Radke, C. J. 1987 Snap-off of gas bubbles in smoothly constricted noncircular capillaries. *AIChE J.* **33**, 753–765.

Ratulowski, J. & Chang, H. C. 1989 In snap-off at strong constrictions: effect of pore geometry. In *Surface-Based Mobility Control: Progress in Miscible Flood Enhanced Oil Recovery* (ed. D. Smith), ACS Symposium Series, vol. 33, pp. 282–314. Hemisphere.

Saffman, P. G. & Taylor, G. I. 1958 The penetration of a fluid into a porous medium or Hele-Shaw cell containing a more viscous liquid. *Proc. R. Soc. Lond.* A **245**, 312–329.

Slattery, J. C. 1974 Interfacial effects in the entrapment and displacement of residual oil. *AIChE J.* **20**, 1145–1154.

Smith, M. 1989 The axisymmetric long-wave instability of a concentric two-phase pipe flow. *Phys. Fluids* A **1**(3), 494–506.

Tougou, H. 1978 Long waves on a film flow of a viscous fluid down an inclined uneven wall. *J. Phys. Soc. Japan* **44**, 1014–1019.

Wang, Y. C. 1981 Liquid film flowing slowly down a wavy incline. *AIChE J.* **27**, 207–212.

Wei, H.-H. 2000 The effect of tube corrugation on the stability of a core–annular flow, PhD dissertation, City College of the City University of New York.

Wei, H.-H. & Rumschitzki, D. S. 2002 The weakly nonlinear interfacial stability of a core–annular flow in a corrugated tube. *J. Fluid Mech.* **466**, 149–177.

Yih, C. S. 1967 Instability due to viscosity stratification. *J. Fluid Mech.* **27**, 337–352.